POLITECNICO DI TORINO

Master's Degree in Biomedical Engineering

Politecnico di Torino

Master's Degree Thesis

SEPLab: an EEGLAB Plugin to Compute Somatosensory Evoked Potentials

Supervisors

Prof.ssa Gabriella OLMO

Prof. Vito DE FEO

Dr. Cristina DEL PRETE

Candidate

Micaela DE SIMMEO

July 2024

Summary

The somatosensory system detects changes in the surrounding environment through the five sensory modalities. Somatosensory evoked potentials (SEPs) are electrical signals elicited by the ascending sensory pathways in response to peripheral nerve stimulation. SEPs can be triggered by different sensory stimuli, such as pain, touch, vibration, or mechanical devices, which stimulate specific sensory receptors and elicit modality-specific SEPs. Stimulation of the median or ulnar nerve of the wrist is used to elicit SEPs related to the upper limb, while the SEP of the lower limb is elicited by stimulating the tibial nerve of the ankle or the peroneal nerve at the popliteal fossa.

SEPs are versatile and important tools in various fields, from clinical to research, with possible future improvements in diagnostic and therapeutic procedures. In the clinical field, they are used as intraoperative monitoring during surgery in which the integrity of the somatosensory nerve pathways may be damaged. They are also used to diagnose and monitor numerous neurological diseases, such as multiple sclerosis and peripheral neuropathies, providing critical information on nervous system activity. In neuroscientific research, SEPs contribute to understanding neural plasticity processes and sensory integration mechanisms.

The proposed project aims to develop an EEGLAB plugin for calculating somatosensory evoked potentials (SEPs). EEGLAB is an interactive and opensource MATLAB toolbox for processing continuous and event-related EEGs. In this thesis, a pre-processing chain of EEG data was developed with the following steps: temporal filtering, artifacts corrections with Independent Component Analysis (ICA), epoching and baseline correction, jitter compensation, and extrapolation of SEPs with the averaging technique. The data used to develop the plugin were recorded at Macquarie University with medial nerve stimulation.

Table of Contents

List of Tables

List of Figures

Acronyms

SI
Primary Somatosensory Cortex

CNS
Central Nervous System

PNS
Peripheral Nervous System

CSF
Cerebrospinal fluid

AP
Action Potential

EEG
Electroencephalography

SEP
Somatosensory Evoked Potential

ECoG
Electrocorticogram

LFP
Local Fields Potential

ERP
Event-related potential

EP

Evoked potential

VEP

Visual Evoked Potential

AEP

Auditory Evoked Potential

MEP

Motor Evoked Potential

SII

Secondary Somatosensory Cortex

MS

Multiple Sclerosis

ITI

Inter-Trial Interval

FIR

Finite Impulse Response

LTI

Linear Time-Invariant

IIR

Infinite Impulse Response

ICA

Independent Component Analysis

SNR

Signal to Noise Ratio

IAAFT

Iterative Amplitude Adjusted Fourier Transform

Chapter 1

Introduction to Brain Anatomy

The brain is a structured entity made of numerous components, each of them fulfilling distinct and crucial roles. The brain processes messages from the external environment through the five senses of sight, smell, hearing, touch, and taste, often simultaneously. It also regulates our cognitive processes, including thoughts, memory, and speech, as well as the coordination of limb movements and the operation of numerous organs in the body [1].

1.1 Principles of Brain Anatomy

The brain is composed by the cerebrum, cerebellum and brainstem.

Cerebrum
The cerebrum initiates, coordinates, and regulates movements and temperature.The cerebrum is the largest part of the brain and it is divided in two major parts: the right and the left cerebral hemispheres. The two hemispheres are joined by a bundle of fibers called *corpus callosum* which delivers messages from one half to the other, but they are separated by the great longitudinal fissure [1][2].
The cerebral hemispheres have discrete fissures that split the brain into lobes. Each hemisphere has four lobes [2][2]:

- *Frontal lobe*: it is the largest of the four lobes and it is located in front of the head. It is involved in decision-making, personality characteristics and motor skills. In the premotor area are located the areas planning voluntary movements, while in the primary motor cortex those producing movements.This lobe contains the area associated with speech ability, the *Broca's area*.

- *Parietal lobe*: it is the middle part of the brain. It is responsible for processing pain and touch in the body, in addition to being involved in comprehending spatial relationships and for identifying objects. *Wernicke's area* is located in the parietal lobe and it helps the brain interpret spoken language.
- *Occipital lobe*: it is located in the back of the brain. The occipital lobe is responsible of visual information, such us colors and shapes.
- *Temporal lobe*: it is located at the side of the hemisphere. It is involved in short-term memory and speech. Its back part is related to comprehend the emotions and behavior of others people.

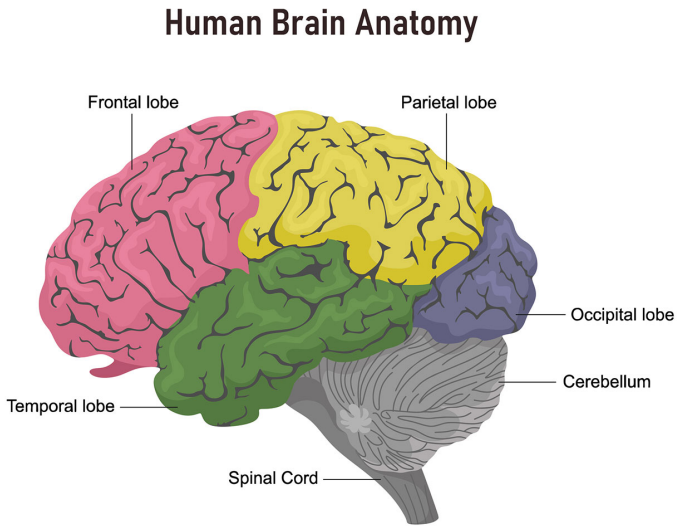

Figure 1.1: Brain anatomy. The brain is divided into three parts: cerebrum, cerebellum, and brainstem. Each hemisphere of the cerebrum may be split into four lobes. Taken from [2]

Cerebellum

The cerebellum is located in the rear of the head, above the brainstem and below the occipital and temporal lobes. The tentorium separates it from the cerebrum. Balance, maintenance of posture and coordination of muscle movements are the functions linked to the cerebellum. Furthermore, it plays an essential role in one's capacity to do quick and repeated tasks. It is divided in two hemispheres, as the cerebral cortex. Neurons are incorporated in the outside region, whereas the inner region establishes contact with the cerebral cortex [2][3].

Brainstem

The brainstem is the lower extension of the brain and it connects the cerebellum and the cerebrum to the spinal cord. The pons, midbrain and medulla oblongata are the three structures that compose it. The pons is responsible for the facial sensation and movements and for the coordination of the eye. The midbrain is involved in the ocular mobility and the medulla oblongata regulates blood pressure, heartbeat, swallowing and breathing. The pons and brainstem carry messages from the cortex to the spinal cord and the nerves that branch from it [1][2].

The cerebral cortex contains [4]:

- *Motor area*: governs the voluntary movement and comprises the premotor cortex and the primary motor cortex.
- *Sensory area*: embraces inputs from the thalamus and processes information about the senses. This area allows the correlation between sensations and specific stimuli. The sensory area incorporates the somatosensory cortex of the parietal lobe, the visual cortex of occipital lobe, the auditory cortex of the temporal lobe and the gustatory cortex.

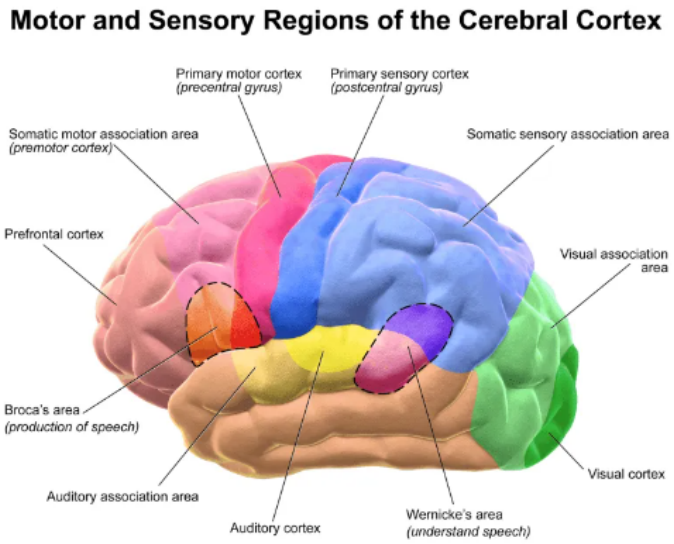

Figure 1.2: Sensory and Motor areas. Taken from [5]

1.1.1 Somatosensory Cortex

The *somatosensory cortex* is related to the reception of sensory stimuli. A somatotopic map called the *sensory homunculus* is associated with the somatosensory

cortex. The homonculus is a disproportionate representation of the human body, in which the size and order of the different areas of the body are directly proportional to the density of skin receptors present (e.g. the mouth and fingers are large). This somatotopic representation of the human body was developed by Wilder Penfield in the 20th century [6][7].

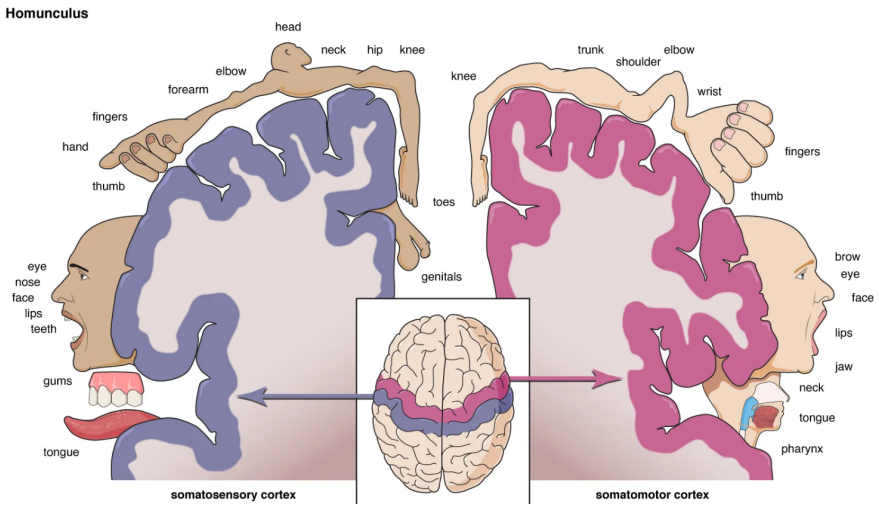

Figure 1.3: Homonculus: somatotopic map of the cerebral cortex.
Somatosensory homunculus: the size of the area is proportional to its importance for sensory perception.
Motor homunculus: the size of the body part is directly proportional to the fineness and precision of the movement. Taken from [8]

The *Primary Somatosensory Cortex*, also know as area SI, is located in the telencephalic cortex posterior to Rolando's cleft (or central) and expands to Silvio's cleft. The primary somatosensory cortex corresponds to area 3b according to Brodmann's classification and is bordered anteriorly by the primary motor area, and posteriorly by the associative areas of the temporal and parietal lobe and the secondary sensitive areas. In the postcentral gyrus there are areas 3a, 1 and 2 that also process somatosensory information and also areas 5 and 6 in the posterior parietal cortex [6]. In particular:

- *Area 3a*: receives proprioceptive information from the Golgi tendon organs and the neuromuscular spindles, which include the state of tension in the joints and thus inform the brain of the state in which the body is in space. In addition, this area projects afferent fibres to area 4 (primary motor area) in order to integrate proprioceptive information with that relating to the will to move;

- *Area 3b*: receives somatosensitive information (e.g. temperature, pain, pressure, fine and coarse touch) and sends it to area 1 efferent fibres relating to the texture of objects and area 2 relating to size and shape.

The somatosensory cortex is composed of six layers like the other areas. In particular most afferent fibers project to the IV layer (inner granular layer and it is more developed than area SI) starting from the periphery (through the thalamus). In contrast, in area 3 the thickest layer is III because of the many efferent fibers to other areas of the cortex and the presence of the pyramidal layer.
Specifically, first-order neurons receive sensory information in the periphery and transport it into the medulla, where a synapse with second-order neurons occurs. These emerge from the gray matter in bundles forming the dorsal columns by joining. Then at the level of specific thalamic areas called nuclei the second-order neurons makes synapse with the third-order neurons that directly innervate the somatosensory cortex [6].
The main functions performed by the SI area are:

- localization of the peripheral stimulus;
- evaluation of stimulus intensity;
- recognition of the shape of objects;
- proprioception.

In addition, sensory information is transferred from the limbs to the somatosensory cortex through sensory pathways. The action potential is transferred from the sensory receptor, which may belong to the thermoreceptor, mechanoreceptor or nociceptor family, to the cortex. Depending on the type of stimulus carried, fiber thickness, different velocity, and the messenger used at the synapse, somatosensory pathways are made to diverge [6][7].

1.2 Nervous System

The nervous system is a complex network of cells known as neurons. Their role is to transmit electrical and chemical signals to deliver motor commands to target muscles and to gather sensory information from receptors [1][2][3]. The nervous system is divided into two main parts:

- *Central Nervous System (CNS)*: it processes the received information and generates appropriate responses. It is composed by the brain and the spinal cord, both shielded by the skull and the meninges, consisting of three layers of tissue known as the *Dura Mater*, *Arachnoid*, and *Pia Mater*. Additionally, the

Cerebrospinal fluid (CSF) acts as a cushion against injuries, removes waste and impurities, and supplies nutrients;

- *Peripheral Nervous System (PNS)*: it detects internal and external stimuli and transmits the responses formulated by the CNS. It comprises spinal nerves emanating from the spinal cord and cranial nerves extending from the brain. The PNS can be categorized into the somatic nervous system, which manages voluntary movements and sensory perception, and the autonomic nervous system, which regulates involuntary functions such as heartbeat, digestion, and respiration.

The CNS is composed by two types of cells:

- *Neurons*: basic functional units of the nervous system. Neurons transmit information over long distances through chemical and electrical signals.

- *Glia*: brain cells that nourish, protect and maintain neurons.

Glia are present in a greater number than neurons, around to fifty to one [9]. A neuron is composed by three parts:

- *cell body*: containing nucleus, which governs the cell's activity. In this cells it is also located the cell's genetic material;

- *dendrite*: stretch from the neuron cell body and receives information from other neurons. The dendrite are lined with synapses, which are the sites two neurons connect;

- *axon*: it spreads from the cells body and ends at nerve terminals and transmits signals from the cell. The axons are covered by a myelin sheath. It covers and shields the axon, enabling the electric impulse to travel more quickly.

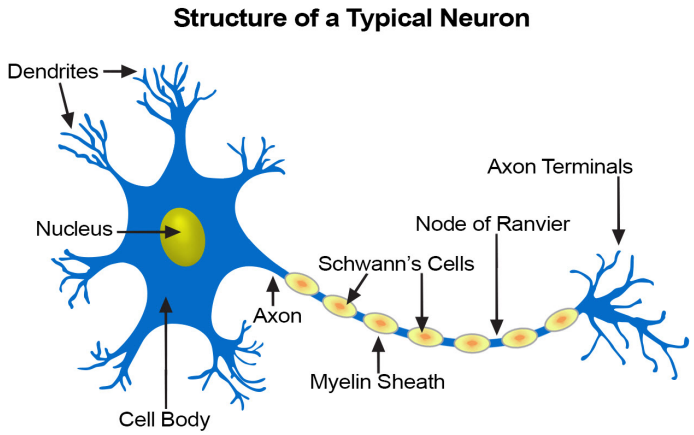

Figure 1.4: Schematic illustration of a neuron. Messages from dendrites move up the axon and are transferred to other neurons via synaptic connections. Taken from [10]

The neurons can be divided in three classes [9][11][12]:

- *Sensory motors*: transmit information from the sense organs to the CNS for processing;
- *Motor neurons*: manage voluntary muscle actions and transmits instructions from nerve cells in the brain to muscles;
- *Interneurons*: are engaged in processing information and they are contained in the CNS. Interneurons are the most prevalent type of neuron.

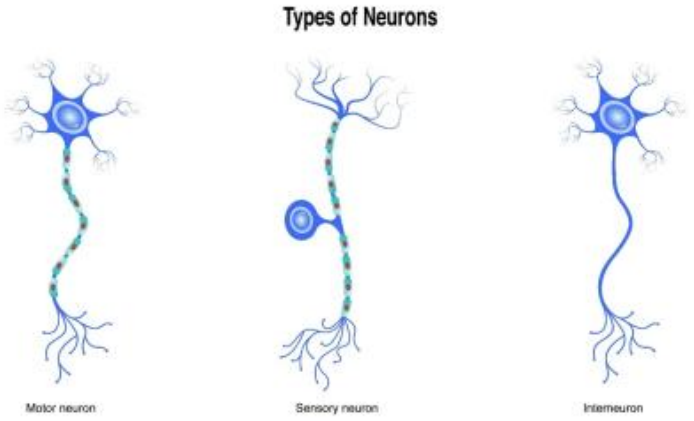

Figure 1.5: Types of neurons. Taken from [9]

1.2.1 Action Potential

Neurons exchange information through electrical and chemical signals. The electrical signals, which allows the communication between neurons is the *action potentials (AP)*.
The cellular membrane and ion distribution, notably sodium (Na^+) and potassium (K^+), play a crucial role in the production and propagation of action potentials. In rest condition, the concentration of the chemical species varies. In particular, the concentration of K^+ ions is higher inside the cell, whereas Na^+ ions are higher outside. The difference in ion concentrations causes a voltage differential, known as resting potential, which is typically around -70 mV and the activity of the Na^+-K^+ pump maintain the equilibrium.
The concentration gradient of each ion creates a flow across selective channels, which are voltage-dependent (depending on the potential difference they open or close), permitting chemical species to traverse the cell membrane. An AP is induced by a quick change in membrane potential, in particular when the sum of the inputs causes the membrane potential to reach a value equal to -55 mV, this is the *action potential threshold*. Specifically the sodium ions flow into the cell as the Na^+ ion channels voltage-dependent open. The difference voltage increases and when it reaches the peak the re-polarization phase starts. In this phase the sodium channels are close whereas the potassium channel are open. During this phase there is an absolute refractory period, in which the neurons can't generate a new action potential, followed by a relative refractory in which if the stimulus received is strong enough the neuron can elicited a new AP. Finally the action of the sodium - potassium pump reestablishes the start condition, the voltage recovers to the value of -70 mV, only after the hyperpolarization process in which the voltage decreases below the resting potential [13][14][15].

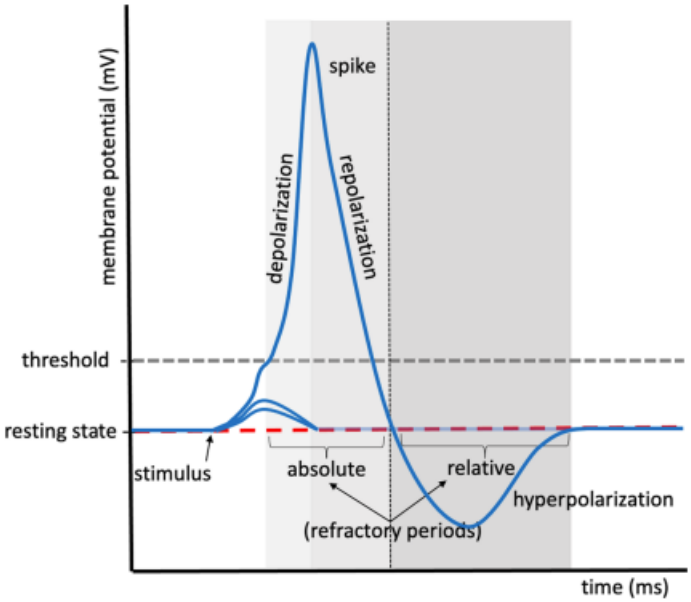

Figure 1.6: Action potential. Taken from [14]

The information exchange between cells occurs through the connection called synapses. The neuron releases a neurotransmitter (the chemical signal) into the synaptic cleft when the presynaptic terminal is reached by an action potential. The transmitter will bind to the neurotransmitter receptor after crossing the synaptic cleft. It will induce a movement of positive (e.g. Na^+, K^+, Ca^+) or negative (e.g. Cl^-) ions through the membrane channels depending on the type of neuron that released the neurotransmitter [15].

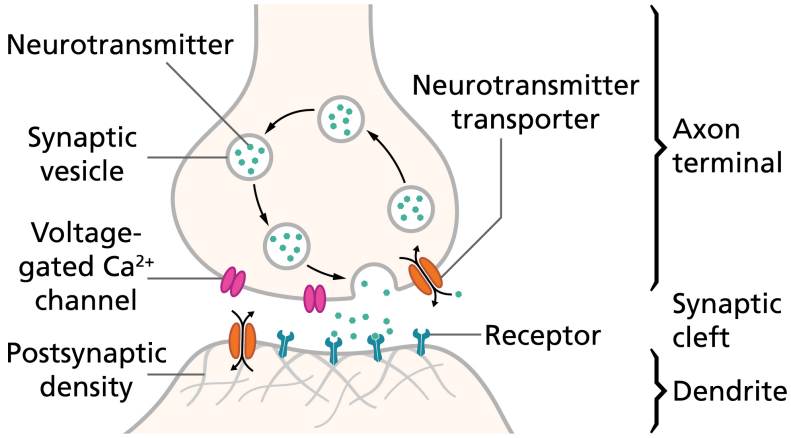

Figure 1.7: Neurotransmitter is released from the neuron into the presynaptic cleft (20-40 nm gap between the presynaptic axon terminus and the postsynaptic dentrite) when the action potential reaches the presynaptic terminal.
Synapses convert an electrical signal (action potential) into a chemical signal (neurotransmitter). They then convert the signal back to electrical form after the neurotransmitter has bound to the postsynaptic receptor. Taken from [15]

Chapter 2

Somatosensory Evoked Potentials

2.1 Biosignal: Electroencephalogram

Electroencephalography is the field focused on recording and interpreting electroencephalogram signals. The electroencephalogram (EEG) represents the time course of extracellular field potentials generated by synchronous neuronal activity. In 1875, the first recordings were made on animals by Richard Caton and it was not until 1924 that electrical activity was recorded on humans by Hans Berger [16]. EEG can be measured using electrodes positioned directly on the cortex or on the scalp. In the first case it is referred to as *electrocorticogram (ECoG)* and the measured of the electric fields are known as *Local Fields Potentials (LFP)*. EEG recorded without an external stimuli is termed spontaneous EEG, while it is called *Event-Related potential (ERP)* if EEG is generated in reaction to an internal or external stimuli [17]. EEG signals are crucial for diagnosing and understanding various neurological conditions, including epilepsy, sleep disorders and brain injuries. A normal subject's awake EEG recorded with scalp electrodes has an amplitude of 10-100 µV, while in epilepsy, EEG amplitudes can rise by nearly an order of magnitude. The amplitudes vary from 10 µV to 100 µV when the activity is measured on the scalp, while it is approximately 300 µV or greater in case of ECoG [16][17][18].
The frequency spectrum of the EEG ranges from 0.1 Hz to 100 Hz and is separated into bands that correspond to various behaviors and brain states:

- *Delta waves (0.5-4 Hz)*: are the slowest brain waves. They have high amplitudes (75-200 µV) and great coherence throughout the scalp and are typical for deep sleep (not REM), people in vegetative states and newborns;

- *Theta waves (4-8 Hz)*: are characterized by high amplitude. This rhythm is not present in adults, but can be caused by hyperventilation. Theta waves are associated with tiredness and deep concentration states, they are linked to subconscious activity;
- *Alpha waves (8-13 Hz)*: are predominant in the occipital lobe of the brain and indicate the relaxed state of mind and are connected to the closure of the eyes. Attention and mental effort can block or reduce these signals. Although Mu rhythms share a frequency range with alpha rhythms, they differ in topography and physiological importance. Motor functions block Mu rhythms;
- *Beta waves (13-30 Hz)*: are associated with conscious behaviors, a state of concentration and anxiety;
- *Gamma waves (30-100 Hz)*: has a complex role in brain function, such as the combination of information from two distinct sensory inputs. They are also used to diagnose some brain disorders.

Slower cortical rhythms indicate idleness, while faster rhythms indicate information processing [17][19].

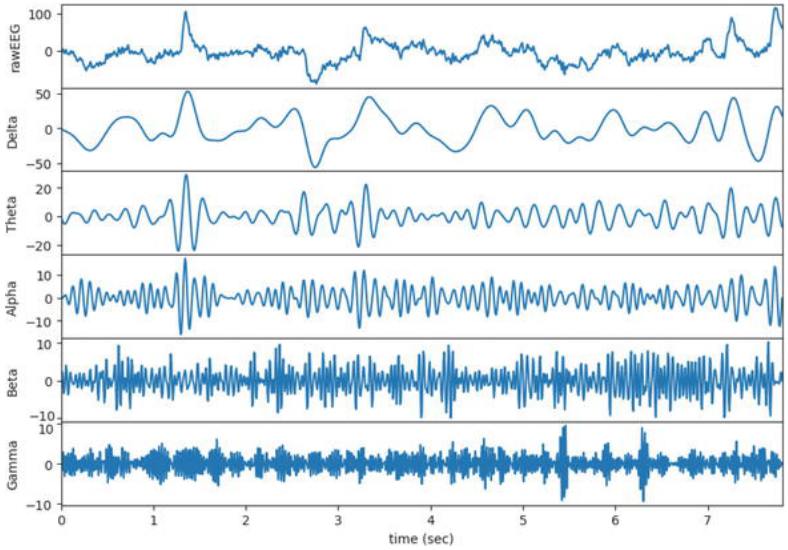

Figure 2.1: Raw EEG data and frequency bands: delta (0.5–4 Hz), theta (4–8 Hz), alpha (8–13 Hz), beta (13–30 Hz), and gamma (30–100 Hz). Taken from [19]

2.1.1 International 10-20 System

The international 10-20 system is the standard for EEG electrode placement and for correlating external skull locations to underlying cortical areas. It was invented

by Herbert Jasper in 1958 to overcome the problem of variability in skull shape and size from person to person.
The electrodes are placed according to ideal lines (antero-posterior midline and latero-lateral coronal line) drawn from repere points:

- *the inion*: external protuberance of the occipital bone;
- *the nasion*: small depression immediately above the nose;
- *the preauricular points*.

The electrodes are placed at a distance of 10% or 20% of the total length of the line from each other. The position of each electrode is recognised using a letter that identifies the underlying cortex region (Fp - Frontopolar, F - Frontal, C - Central, T - Temporal, P - Parietal and O - Occipital) and a number indicating the lateralisation (odd-left, even-right and 'z' for the central line).
The number of electrodes used for recording depends on the device. An EEG with 128 or 256 channels has a high spatial resolution, in comparison, an EEG with 14 channels has a low spatial resolution [19].

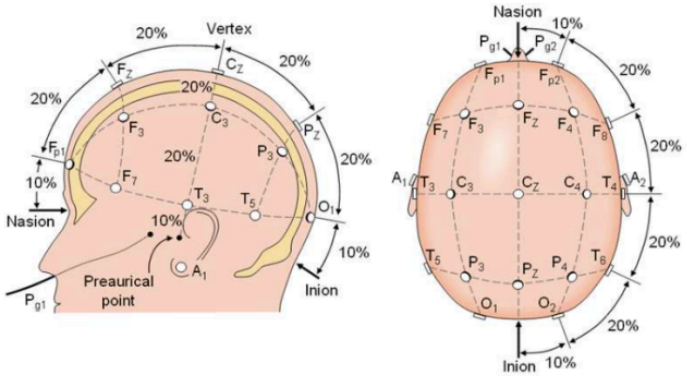

Figure 2.2: International 10-20 System: representation of electrode position on the scalp.
Fp - Frontopolar, F - frontal, C - Central, T - Temporal, P - Parietal, O - Occipital

2.1.2 Evoked potentials

Evoked potentials (EP) describe a specific change in the bio-electric signal following a motor event or stimulation of a sensory pathway. It is characterised by a waveform consisting of positive or negative deflections defined as components. They indicate the presence of synchronous postsynaptic potentials (excitatory or inhibitory) of a group of cortical neurons, that generate a field large enough to be recorded on

the surface, and by localising them it is possible to identify, following a particular stimulus, which cortical area is active. The amplitude of the EP is around 1-3 µV and it is an order magnitude lower than the spontaneous activity. In order to identify them within the EEG activity, the averaging technique is used to reduce the background noise of the EEG. The averaging approach relies on hypothesis such as random background noise, predictable and repeatable EP and the EP and the EEG are independent [18].
In the study of the evoked potentials, the parameters analysed are:

- *Amplitude*: magnitude of component deflection compared to the basal level (i.e. value at rest in the absence of stimulus or standard events;
- *Latency*: it is the delay between the presentation of the stimulus and the appearance of the response;
- *Topography*: position on the skull surface where the maximum amplitude of the component is recorded;
- *Polarity*: it depends on the distribution of the electric field produced by active cortical areas and on the position of the electrodes on the scalp. The polarity defines whether the component has a positive or negative sign.

The Evoked Potential are divided in two categories [16][20]:

- *Stimulus - Related*: depends on the physical characteristic of the applied stimulus (i.e. for the auditory system are the intensity and tone, for the somatosensory system are the stimulation mode and the intensity);
- *Event Related Potentials (ERP)*: depends on the psychological context in which the stimulation takes place. Compared to correlated stimulus potentials, ERPs are information-dependent and arise only when the subject pays attention to and assigns significance to the stimulus. In the field of neuroscience, ERP signals allow us to understand the correlation between brain activity and its manifestations in subjective behaviour and experience.

ERP Components

ERP components are an explanatory neurophysiological reflex of the brain's information flow, as they are capable of convey details concerning the reception and low-level processing of sensory stimuli, as well as processing at a higher level. The nature of the components of the ERPs, which occurs at different time, is distinct. They are known as *early* and *late ERP*. The *early ERPs* are associated with receptor and peripheral nervous system responses. They have a latency around 10-20 ms and are known as *far fields*. The brain generates *late ERPs*, known as *near-field*

potentials. The late ERPs are subdivided in two components: exogenous and endogenous. The *exogenous* components are influenced by the physical and sensory external stimulation (visual, motor, auditory). They reach a peak in the first 100 ms post-stimulation. The *endogenous* components are affected by attention to the stimuli, reflect higher-level processes. They have a latency over 100-200 ms [17][21]. The components of the ERP relate to numerous brain processes and are obtained from brain activity recorded on the scalp. In the following, the main ERP components are briefly explained in relation to their location on the scalp and their possible functional significance:

- **P100:** its latency is 50 ms if the stimulus is auditory and 100 ms if it is visual. The P100 is a positive peak and it is not always easily identifiable. In the visual stimulus the P100 reaches the maximum amplitude in the occipital regions, while reaching the maximum amplitude in the central and frontal regions in the case of an auditory stimulus (the component propagates from the posterior area of the scalp).
  The P100 component is considered as a neurophysiological measure of attention to a sensory stimuli, providing insight into the sensory channel's integrity [20][21];

- **N100:** reflects the pattern recognition process and the attention to the characteristics of the stimuli. It is a negative wave. In the visual stimulus the latency is around 150-200 ms. The maximum amplitude can be reach in the parietal cortex or in the central areas of the cortex. The N100 auditory has two component the first one has a latency of 100 ms and it is on the central areas, the second one has a latency of 165 ms and it is on the parietal areas. The intensity is lower if the stimuli are presented in a short time between each other;

- **P200:** has a latency of about 200 ms and has positive polarity. It is associated with cognitive tasks, such as short-term memory and selective attention. P200 together with N100 is present in auditory stimuli (low-frequency or high-frequency sound), but is sensitive to the parameters of the stimulus provided and is less localised on the scalp. Maximum amplitude is recorded near the frontal regions. In the case of visual stimuli, the P200 occurs with a latency between 150 and 275 ms and the greatest amplitude is recorded at the frontal area [21][22];

- **N200:** component with latency of about 200 ms and with negative deflection. The greatest amplitude is recorded at the fronto-central region. It is associated with target selection and stimulus discrimination. The amplitude and duration are reduced if to reduce the inter-stimulus interval, also it is characterized by

low repeatability because it varies greatly among different individuals. The N200 is divided into three components:

  - *N200a:* has a latency between 100 and 250 ms. It is related to paradigms characterized by variable stimuli, different from each other;

  - *N200b:* is elicited when changes in the physical properties of the stimulus are important to the task and it is later than the N200a component;

  - *N200c:* is evoked when there is a requirement for classification and discriminating among diverse stimuli [23].

- **P300:** is an endogenous component that occurs with a latency of about 300 ms. It is related to discrimination and recognition of rare stimuli, called targets. The latency is related to individual cognitive ability and depends on the speed of stimulus classification: for known stimuli it is lower. P300 amplitude is considered a manifestation of central nervous system activation reflecting attention to the incoming stimulus as memory representations are updated. It is related to the distance between two targets stimuli and the rarity of the stimulus. The amplitude is greatest in the median centro-parieto-occipital area [17];

- **N400:** peaks around 400 ms, but has a latency between 250-500 ms. It has maximum amplitude on the centro-parietal electrodes and for visual stimuli is slightly greater on the left side. The N400 is related to brain response to words and other significant symptoms, such as pictures, faces, and language signs;

- **P600**: has the onset at about 500 ms and peaks at 600 ms after the stimulus and has a duration of several hundred milliseconds. It is related to processes associated with language and memory processes. P600 can be elicited through auditory and visual tasks. It appears under the centro-parietal electrodes, but some studies have also observed frontal P600 presenting.

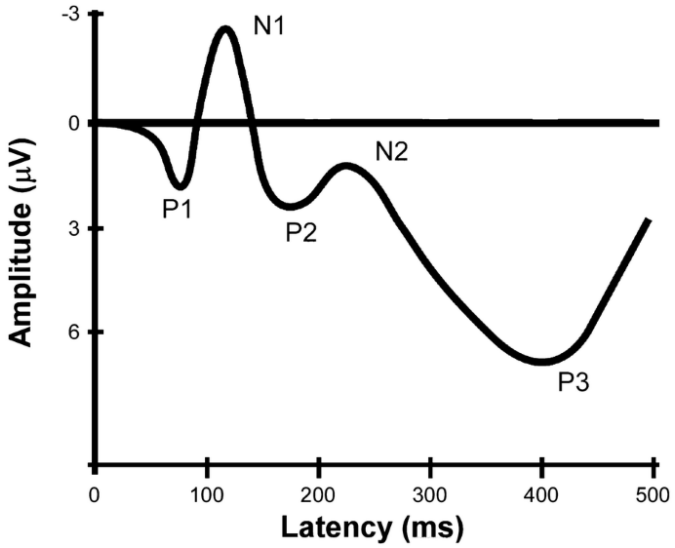

Figure 2.3: Example of a Event Related Potentials and its components. Taken from [24]

Type of ERP

The ERPs can be classified on the base of the sensory organ that is stimulated: Visual Evoked Potential (VEP), Auditory Evoked Potential (AEP), Motor Evoked Potential (MEP) and Somatosensory Evoked Potential (SEP).

The **Visual Evoked Potentials** are used for investigate the functional integrity of the anterior visual pathways, for diagnosis and management of patients with neurological disease. In particular, it is helpful in patients with disorder which involves the visual pathways without visual symptoms, and for patients with visual symptoms. However there were no objective results throughout the examinations. VEPs give an objective and reproducible measure of visual function and are used to assist solve clinical problems. The VEPs are elicited by repetitive visual stimuli, which could be patterned or unpatterned achromatic stimuli presented monocularly. The unpattened stimuli is made of brief bursts of white light, while the pattern stimuli usually use a checkerboard patterns in which are alternate dark and light square, or alternate sinusoidal grids or bars. For detecting pathology of the optic pathways the VEPs elicited by pattern reversal is a bit more sensitive than the VEPs elicited by flash [25].

The **Auditory Evoked Potentials** are elicited by a response to click, which evoked the brainstem response. AEPs evaluate the course of the acoustic nerve to the brainstem. They are also know as *Brainstem auditory evoked responses*

(BAERs) or *Braistem auditory evoked potentials (BAEPs).* Operating monitoring and audiology is where AEPs are generally applied [26].

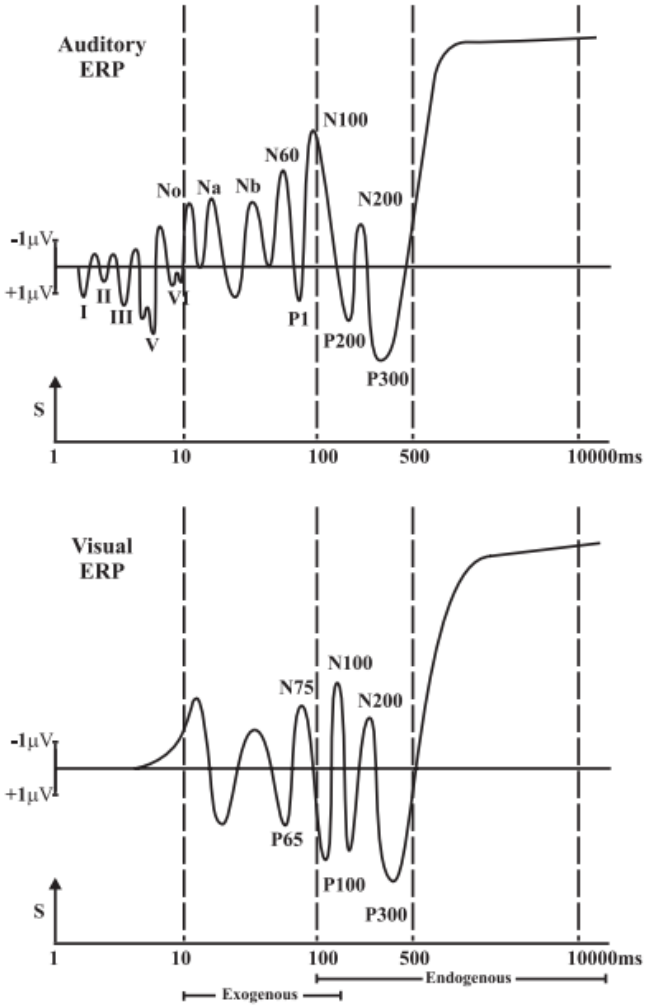

Figure 2.4: Representation of Auditory Evoked Potential and Visual Evoked Potential in logarithmic time scale with Commonly recognizable components. The components of the AEP represented by roman numerals are the brainstem evoked potentials. Endogenous components are comparable in both modalities, while exogenous components have modality-specific characteristics. Taken from [17]

The **Motor Evoked Potentials** are measured peripherally in response to a magnetic or cortical stimulation. These evoked potentials allow us to analyze the pathway that leads the stimulus that starts in the cerebral motor cortex and through

the spinal cord reaches the motor neurons and ultimately to the muscles. MEPs are typically utilized in conjunction with SEPs to monitor spine surgical procedures [26].

The Somatosensory Evoked Potentials are described in detail in the following section.

2.2 Somatosensory Evoked Potential

The **Somatosensory Evoked Potentials (SEPs)** are presynaptic and postsynaptic reactions recorded throughout the spine, limbs and scalp after the stimulation of peripheral mixed sensory and motor nerves or cutaneous sensory motor. Somatosensory stimulation has always been associated with EEG; over time we have moved from using single electrodes with poor signal quality to electrodes that apply critical adaptations such as real time filtering, shielding and post-processing in order to produce good quality signals. The evaluation of sensory transmission in the proximal peripheral nerves, spinal cord, and brain is the primary use of the SEPs. The main applications of SEPs are:

- to investigate the central somatosensory pathway;
- Identifying anomalies in the spinal cord, brain stem, or cortex in disorders such multiple sclerosis or cervical stenosis;
- To supply objective evidence of CNS dysfunction when sensory symptoms are ambiguous and neurologic evaluation is normal;
- To help identify sensory symptoms to the proximal peripheral nerve (roots), spinal cord, or brain.

Electric stimulation consistently elicits larger amplitude evoked potentials than physiologic stimuli like finger taps or tendon stretches, making it the sole suitable stimulus for clinical usage [17][27]. In the clinic, the study of the somatosensory evoked response of the lower limbs (tibial and peroneal nerves can be stimulated) and upper limbs (median nerve or ulnar nerve is stimulated) is relevant. SEPs depend on many factors and not only on the stimulation protocol, such as the intrinsic characteristics of the stimulation site, the number of receptors and their receptive field. An understanding of the neural pathways and structures involved in stimulation is important to better understand somatosensory evoked responses.

2.2.1 Somatosensory Processing Pathway

SEPs can be induced by mechanical or electrical stimulation. Electrical stimulation bypasses mechanotransduction mechanisms by activating large diameter, fast-conducting type Ia muscle and type II skin afferent fibres. In contrast, when a mechanical stimulus is presented, the phenomenon of sensory transduction occurs. With this type of stimulation, changes in the ionic permeability of the neural structure underlying the skin are induced to originate a depolarizing afferent current that is decoded in the brain and translated into sensation. As a result, the SEPs have different latencies between the two stimulations, in particular due to the lower conduction velocity of skin afferents for mechanical stimulation and the indentation of skin and mechanoelectric transduction in skin receptors [28][29].
The somatosensory system is divided into two parts [Figure 2.5]:

- *Spinothalamic system*: is responsible for visceroception, nociception (pain and impending tissue damage), and thermoreception (heat and coolness). It is also known as extralemniscal system;
- *Dorsal column–lemniscal system*: is responsible for proprioception (e.g. joint movement, position, and strength) and mechanoreception (vibration detection, contact localization, and tactile object recognition).

Both systems can be divided into four different neuronal populations. In the dorsal root ganglia, the trigeminal nucleus of the midbrain, the trigeminal ganglion, and the vagal nodose ganglion are situated in the somata of the first-order neuron. In contrast, those of the second order are located either in the spinothalamic tract system (in the dorsal horn of the spinal cord) or in the limniscal system (in the nuclei of the dorsal column). The systems project to the third-order neurons (ventroposterior nuclei of the thalamus) which in turn transmit to the network of somatosensory cortex (i.e. primary and secondary somatosensory cortex, mid-cigulate cortex, medio-superior and posterior cortex, and posterior parietal cortex) to the neurons of order four. The function of the dorsal column-lemniscal system is what is assessed by the standard techniques of SEPs. Somatosensory system impairment is provided by the presence of abnormalities in SEPs, but selective impairment of the spinothalamic system is not excluded by findings of normal SEPs [30].

The afferent signal from the stimulated area is transmitted to the dorsal root ganglion cell, which in turn projects it through the dorsal root of the cervical spinal cord and their their axons form synapses with the brainstem nuclei in the caudal cord. The second neuron's axons travel across the midline and project to the ventroposterior thalamus via the medial lemniscus. The ventroposterior thalamus (VPL) is accessible via fibers in the medial lemniscus. The VPL then sends signals

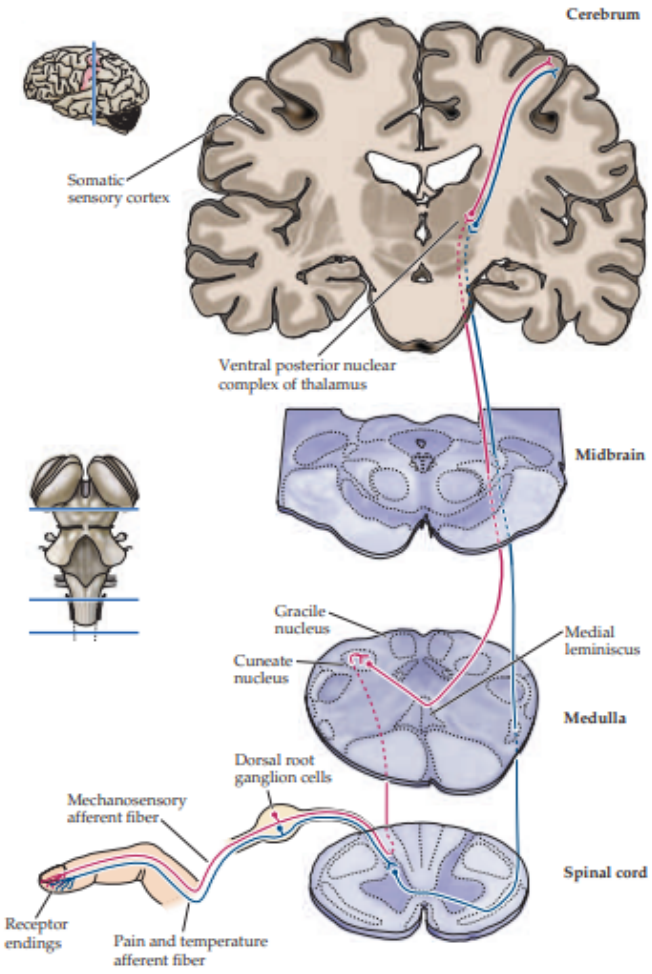

Figure 2.5: A schematic representation of the somatosensory system. The somatosensory system is composed by two primary parallel pathways. The spinothalamic tract system (blue lines) supports thermoreception, nociception and visceroception. The lemniscal system (pinky lines) facilitates proprioception and mechanoreception. Taken from [31]

to the postcenral gyrus in the primary somatosensory cortex. Regions 3a and 2 of the SI receive propioceptive inputs, whereas regions 3b, 1, and Brodmann's area receive mechanococeptive inputs from the skin. In the primary somatosensory system, tactile object recognition begins by extracting features (e.g. direction of movement, edge detection), and via a ventral stream (involved in tactile recognition) it reaches the secondary somatosensory system in the parietal operculum and insula where object recognition continues. In Brodmann areas 5 and 7 located in the posterior parietal cortex via a dorsal stream (involved in somatosensory-visual

integration) the localisation of the stimulus is processed. Spinothalamic projections reach as terminal groups to the main thalamic somatosensory nucleus (ventrobasal group or Vc) and are distinct areas from the medial lemniscus terminal region. Thalamic neurons with nociceptive input provide signals to the SI, SII (Secondary Somatosensory Cortex), frontal operculum and dorsal insula. Area 1 of the primary somatosensory area is where most of the nociceptive neurons with input from the ventrobasal thalamus are located. While the tactile input in the SII comes mainly from the SI and the halamus provides it with nociceptive input [27][30]. Somatosensory evoked responses are a standard method for identifying brain circuits and structures, as well as highlighting malfunctions. SEPs show a characteristic waveform, with peaks and troughs linked with ascending information reaching a specific brain component.

2.2.2 Characteristic Component

As in evoked responses, the somatosensory signal has a prototypical response characterised by short, medium and long latency components, and the presence of specific components is related to the nature of the clinical protocol. Short latency components are related to cognitive states. In contrast, medium and long latency components of greater amplitude are linked to experiments that require subjects to perform cognitive functions or to be vigilant [32]. The dynamics of the elicited response and the corresponding neural mechanism that generated it differentiate the characteristic components. The ascending information that arrives sequentially in the dorsal root entry zone, medial lemnsic and postcentral gyrus (SI) are early components and have a high frequency content. The activation of the relay nuclei and the change in the conduction of the surrounding volume induce the recorded changes in the electric field. Subsequent components are characterised by low-frequency content and are associated with further processing of the stimulation in the upper part of the sylvian fissure. Neural structures that generate long latency components are characterised by longer refractory periods. Therefore, long latency components are not elicited by high stimulation frequencies, so a low stimulation frequency of approximately 1 Hz is recommended [33][34]. Some components with their respective neural sources are listed in the Table 2.1, but the values depend on various factors, such as age, sleep phase, the subject's mental state, temperature.

Component Name	Generator
P9	Distal brachial plexus
P11	Dorsal root entry zone
P13/P14	Medial lemniscus
N16	Thalamus
P18	Pons/Medulla
P20/N20	Pre/post central gyrus
P22	Supplementary motor cortex
P40-N60	Thalamocortical projections
P45	Parietal region
N60	Parietal region
P65	Myogenic origin
P100	Upper wall of SS in SII (i.e. parietal operculum)
N125-P200	Surface cortex above SII
N140-P200	Corpus callosum/ somatosensory associative cortex/orbitofrontal cortex

Table 2.1: Neural sources and their respective components [33]

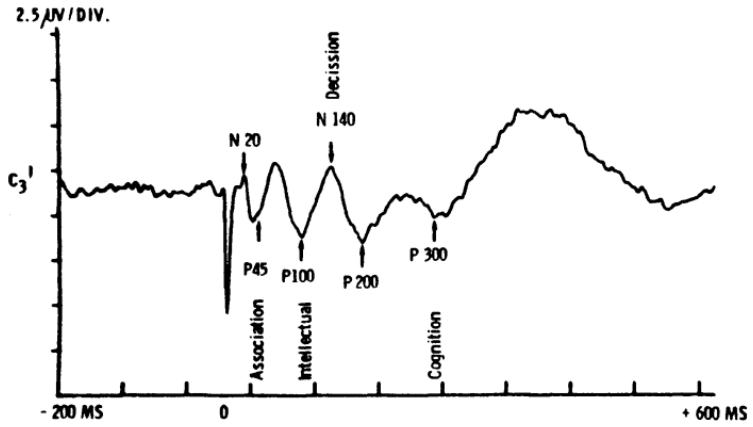

Figure 2.6: A typical long-latency SEP. The right median nerve is stimulated at twitch level. Taken from [33]

2.2.3 Clinical Application and Challenges

SEPs were the first evoked potentials studied on healthy subjects and patients due to their relatively large amplitude and low frequency compatible with a low

sampling rate of the A/D conversion. In 1947, George Dawson recorded the cortical somatosensory response in patients with myoclonus, the first SEP, a neurological condition characterised by involuntary and sudden contractions of a muscular group [35]. Clinical information on the human body's reaction to perception can be revealed by variations in waveform, latency and amplitude. SEPs are exploited to identify CNS lesions when clinical examination findings are equivocal or normal. The amplitude of the potentials is modified by axon disease, while variations in latency are induced by myelin disease. SEPs can act as a support on blood supply information to the spinal column during spinal cord surgery and can predict the outcome of a cardiac arrest. In addition, they can be used for patients with spinal cord tumours. In particular, a reduced amplitude or absence of the N13 component is indicative of grey matter involvement and is linked to reduced upper limb reflexes and disturbances in temperature and pain sensation. In contrast, altered tactile and joint sensation is linked to an abnormality of P14. It also has clinical application for the evaluation of suspected multiple sclerosis (MS). In particular, a SEPs in MS presents normal waveforms and amplitude, but with a longer latency between peaks. Particularly for MS, tibial SEPs, with co-located pathways from the lower extremities, are more likely to exhibit abnormalities than medial SEPs. SEPs recorded in children in coma due to hypoxicischemic encephalopathy, head trauma are similar to those in adults. In particular, a study was conducted on 127 children who were comatose due to severe head injuries, and who did not present an auditory evoked responses of the brainstem and SEPs died. In addition, SEPs are a useful predictive tools for infants with asphyxia, but they also have long-term predictive value for impairments that arise during the school years [27]. Furthermore, in adults, the persistence of the vegetative state in comatose patients in intensive care or the prediction of death can be suggested by the absence of cortical components. In particular, there is a loss of the N20 component, while N13 creates an input signal for the CNS and can still be elicited. But this loss of the N20 component can also occur in patients with: severe cerebral edema, drug intoxication and severe bilateral supratentorial lesions. Recent studies have revealed that the N18 component, formed by the skin nucleus in the caudal medulla near the respiratory center, is lost in brain death but preserved in recordings of comatose but not brain-dead patients [27].

Chapter 3

Experimental Protocol

3.1 Experimental setup

The data used in this thesis were provided from the Macquarie University which are used in a project for studying through the time-resolved multivariate pattern analysis if there is neural overlapping representations between the seen touch and the first-hand experience of touch on EEG data acquired from people with and without vicarious touch experience.

Thirty-four right-handed undergraduate students were selected for the study. No neurological disorders and normal or correct to normal vision are reported from all the participants. For taking part to the study all participants provided written consent and gained $20 per hours or course in return for the involvement.
During the recording, data participants received direct tactile stimulation to their own hand alternating with watching videos representing contact to another person's hand. Tactile trials stimulated the participant's right hand's little finger or thumb, whereas visual trials showed a right hand being touched on the little finger or thumb on a screen. Both the student's hand and the hand on the screen flipped between runs (palm down or palm up) to control for external touch-side (right vs. left), ensuring that touch to each individual finger happened equally frequently on the left and right sides of the screen [36].

The *tactile stimuli* involve the touch of the thumb or the little finger of the participant's right hand. To the top of the fingers, there was attached a round probe (maximun extention: ∼2 mm, diameter: ∼3 mm) which with the two electromagnetic solenoid-type vibrotactile stimulators (height: 12 mm, diameter: 18 mm) produced the touch. The tap has a duration of 500 ms in the normal trials and of 100 ms for the target trials. For maintaining the same trial duration, 400

ms were added to the end of each target trial.

The *visual stimuli* involve videos, length 1825 ms, which show a female right hand, with a dark gray background, in which occurs the touch of the little finger or thumb. At the beginning of each video, there are two pointy metal sticks positioned over the top of the thumb and little finger. One of the stick moved in the direction of one of the finger at the beginning of the video and touched it for 500 ms before withdraw, while the other stick remains stationary the whole time. During the acquisition, twelve different videos are showed in an equal number of times which are obtained from different combinations of spatial position of the hand (palm down and palm up and from the turned the hand slightly clockwise and anticlockwise) with the objective that the classifier wouldn't depend on unnecessary spatial information. For the target trials are showed videos with the same length of the previously but with a shorter touch (100 ms). They added some frames at the end of the videos and removed some frames from the middle of the touch. Every video is made up of 73 frames which were shown in 1825 ms. The 40 frames for second is the sampling rate whereby were presented with a rate of refresh of 120 Hz.

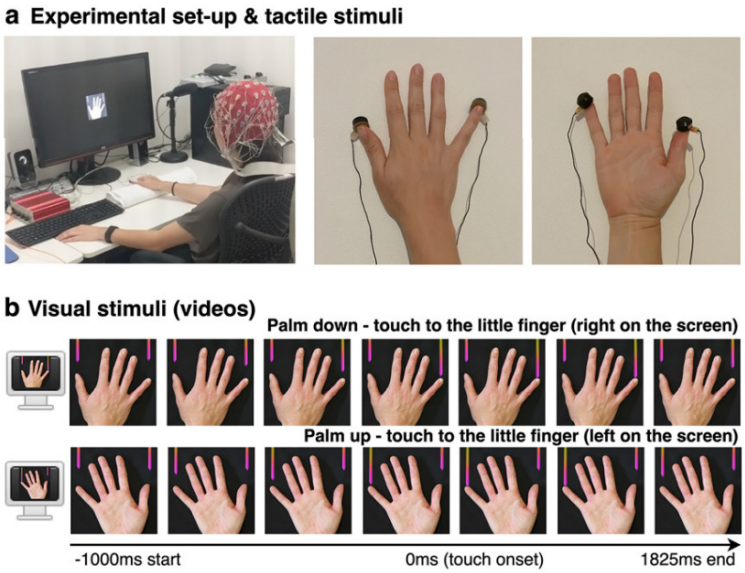

Figure 3.1: Experimental design and stimuli. Taken from [36]

.

3.1.1 Protocol

During the experiment, participants were seated in a poorly lit room in front of a computer screen with their hand placed on the table and aligned with the centre of the screen. Participants wore the EEG cap with the Cz electrode positioned on the vertex and two little tactile devices were placed respectively on the tip of the thumb and little finger of the right hand. A white noise was reproduced through loudspeakers positioned at the sides of the computer screen for covering the possible auditory noise coming from the tactile devices and in addition participants wore earplugs. Throughout the duration of the experiment, subjects were instructed to stare at a white cross fixed in the centre of the screen to reduce eye movements. After completing the set-up before starting the experiment with the space bar, a run test was performed subsequently to verbal and written instructions in order to be sure that the task was correctly understood.
During the acquisition of data, an alternating series of nine consecutive touches (tactile trials) on the hand and nine subsequent touches on the screen (visual trials) were provided. Within each experimental run, the finger touched, the orientation of the hand (the side of external contact), and the modality and frequency with which one trial follows the next were counterbalanced, thus the modality in which a run (visual or tactile trials) begins varies. Each run consists of four blocks, each one with 36 trials. At the end of each block, the orientation of the hand was changed (palm down or palm up) and subjects were instructed by text that the next trial could be another touch to the thumb or to the little finger [Fig.3.2]. The option are: little finger $\rightarrow$ little finger; little finger $\rightarrow$ thumb; thumb $\rightarrow$ thumb; thumb $\rightarrow$ little finger. A finger could be touched no more than four times in succession.

The assignment for the subjects consisted of counting in each block the number of times a shortest touch (target trial) occurred individually for the little finger and for the thumb, in this way the participants paid attention to the finger that was touched. At the end of each block, a question was placed on the screen asking how many short touches the subject had counted to the thumb or to the little finger. Subjects answered on the keyboard with a number from 0 to 9, and after giving their answer they received feedback on whether or not the answer was correct. The counting of the target trials started again from 0 at the beginning of each block.

A total of 12 runs were performed, each one divided into four blocks of 36 trials, in which nine tactile and nine visual trials were alternated. A total of 1728 trials (864 visual and 864 tactile) and a further 240 target trials (20 per run) were performed for each participant. Each run lasted 7-8 minutes, with short pauses between blocks and runs, and with an inter-trial-interval (ITI) of 800 ms between each trials. Participants to continue the experiment pressed the space bar after

checking the duration of each pause.

The whole session lasted about three hours because after data acquisition, the subjects' vicarious tactile experience was assessed by means of a three-part questionnaire. Initially, 10 videos of a *neutral touch*, i.e. neither pleasant nor unpleasant, of a Caucasian female hand on a black background were shown. Next, the participants were asked if they felt any physical sensation on their body and if so, where it was felt. A second question was then asked if they had felt a touch on their fingers during the experiment when the visual stimuli were presented. At the end, to assess emotional responsiveness (a dimension of empathy that concerns the prediction of others' thoughts and feelings) they used a short five question Empathy Quotient scale.

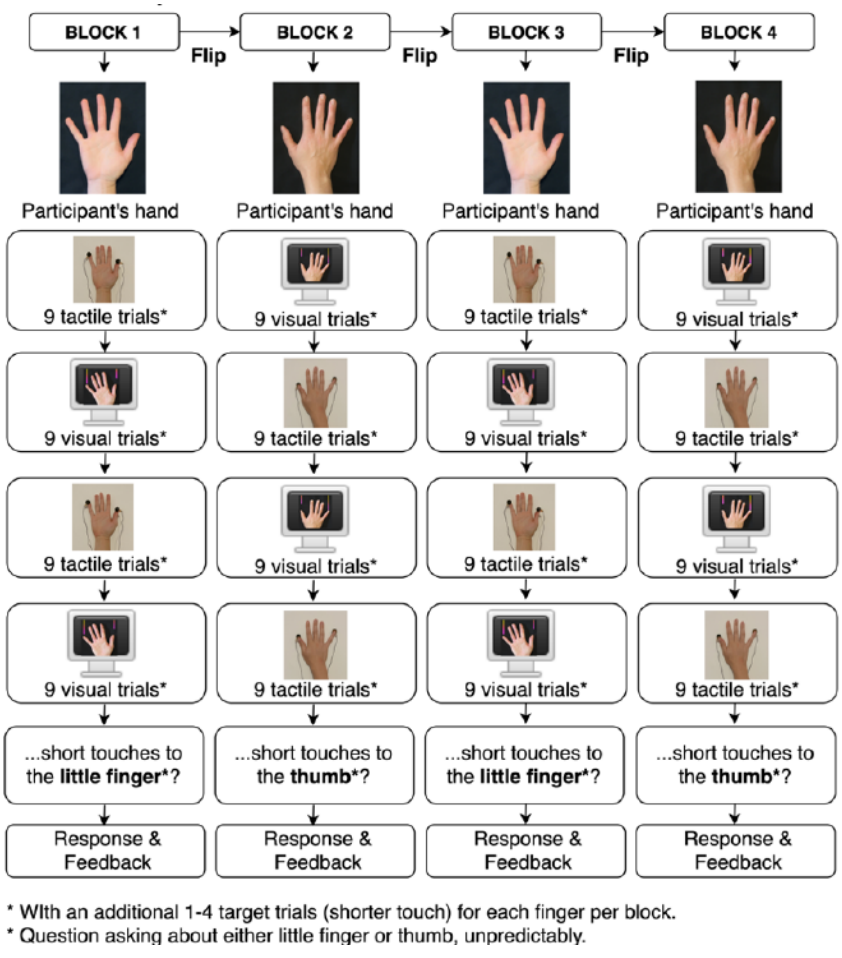

Figure 3.2: Example of run. Taken from [36]

3.1.2 EEG Data Acquisition

The data acquisition was done using a 64-channel Active-Two BioSemi active electrode system at a sampling rat of 2048 Hz. For correcting the high impedances the system uses a pre-amplifier stage on the electrode. The offset voltage was maintained below 20 mV. The EEG system was linked to a Dell Precision T3620 computer running Windows 10 via a fiber optic cable. Data acquisition was overseen using the BioSemi acquisition software on an iMac with macOS version 10.14.1. Electrode placement following the international 10/20 standard [36].

Chapter 4

SEPLAB

EEGLAB is an interactive open-source MATLAB toolbox for processing continuous and event-related EEG, MEG and other electrophysiological data. It was developed by Swartz Center for Computational Neuroscience (SCCN) of the University of California San Diego (UCSD). EEGLAB includes independent component analysis (ICA), time/frequency analysis (TFA), artifact rejection, event-related statistics, and various visualization modes for both averaged and single-trial data. Its graphic user interface (GUI) allows the selection between the different operations. As an open-source platform, research programmers and method developers can share new techniques through 'plug-in' functions that automatically appear in the EEGLAB menu for users who download them [37][38].

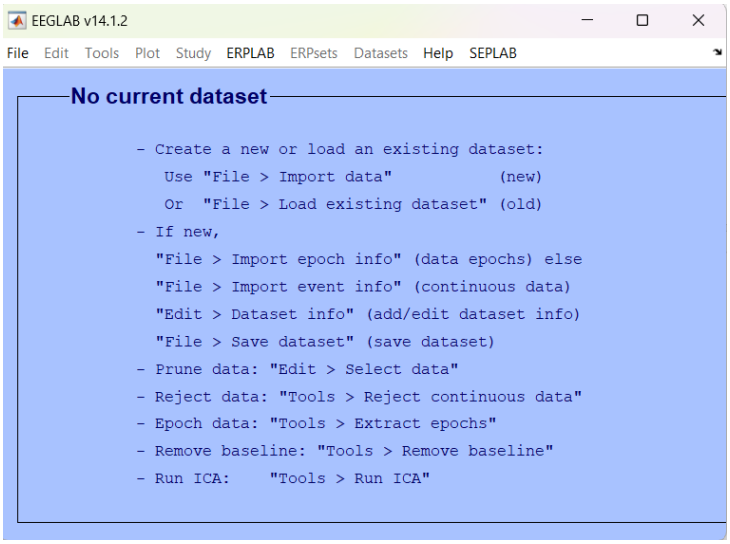

Figure 4.1: EEGLAB interface.

4.1 SEPLAB

SEPLAB is an EEGLAB plug-in developed specifically for the SEP and it is an adaptation of the MRCPLAB plug-in developed for another project. It interacts with and utilizes several EEGLAB functions while also introducing more specific new ones. By running EEGLAB, you can access SEPLAB from its menu, where the different functions are displayed. This chapter will discuss in detail the pre-processing chain implemented to obtain SEPs and the functions implemented in the plug-in.

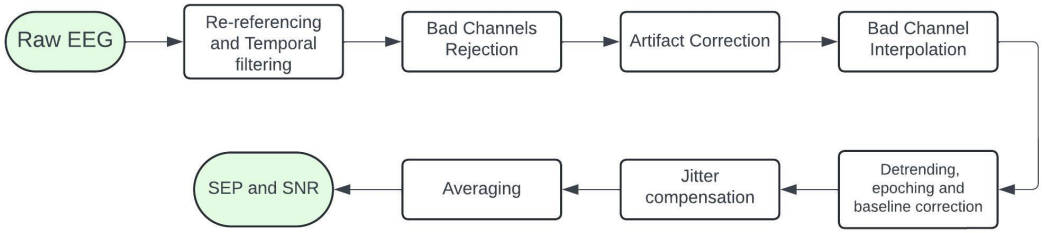

Figure 4.2: SEPLab processing chain for each biosignal.

4.1.1 Import and Save Date

The first step is the import of the EEG data. Therefore the first implemented function relates to the import, the re-referencing and the temporal filtering of the dataset. The extention of the data is *.bdf*. They are imported with this format if they are processed for the first time and then saved in the .set format. The *BDF* format (BioSemi data format) is the native data format for BioSemi recording systems. This format was born out of the need to overcome the limitation of the EDF format that was only able to support int16 values, therefore the BDF format is the 24-bit extension of the EDF format.

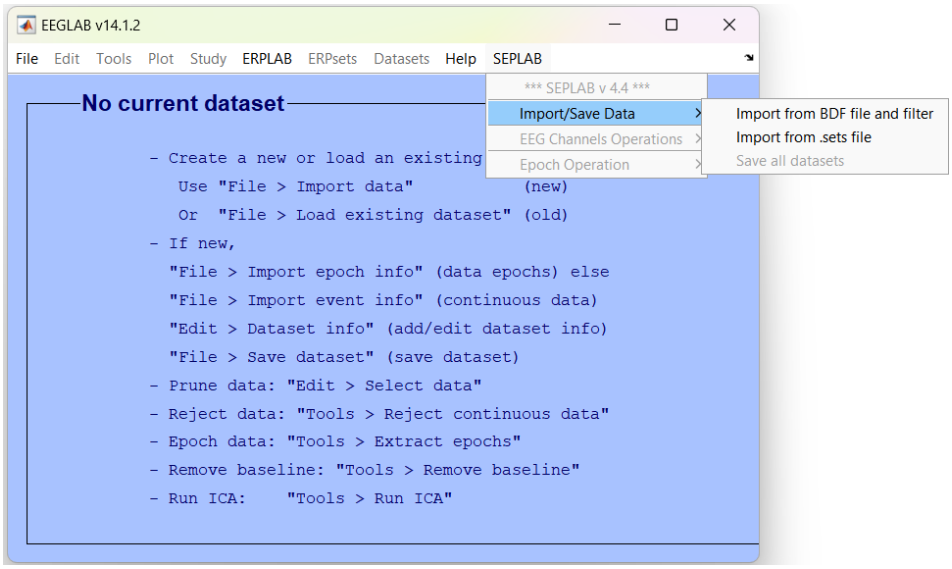

Figure 4.3: SEPLab and 'Import/Save Data' Menu.

If the option *Import from BDF file and filter* is selected, the plug-in opens a window asking the user to enter some information:

- *Subject:* the number corresponding to the subject whose data has to be processed;
- *Sampling frequency*;
- *Number of sessions:* the number of sessions acquired during the experiment. If the number of sessions is greater than 1, they will be merged;
- *Number of channels:* the number of channels used in data acquisition.

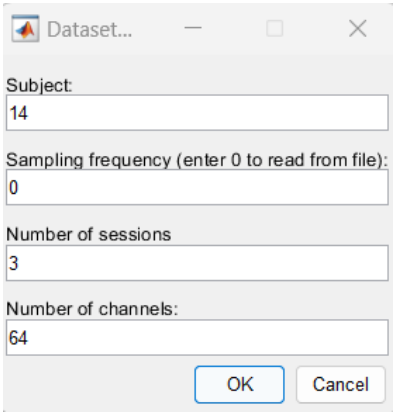

Figure 4.4: Dataset parameters settings while importing datasets.

Re-referencing

The reference electrode's location on the skull clearly affects the signal recorded on each channel, and any noise (such as contact noise) added to the electrode affects all measured signals. Re-referencing to the common average is performed, subtracting the average of all electrodes, to reduce the dependence on the position of the reference electrode. This eliminates common noise and non-specific global potentials, and improves the detection of local activity [39].

$$m(t) = \frac{1}{N} \sum_{n=1} x_{\mathrm{n}}(t) \tag{4.1}$$

where m(t) is the average removed from the channels.

Temporal Filtering

A well-known preprocessing step in electrophysiological research is filtering. Its purpose is to remove or attenuate frequency components present within raw signal improving the signal to noise ratio. However, it can remove useful information from the signal or distort it if not used with caution. The filters are divided into two groups:

- **FIR (Finite Impulse Response)**: are random Linear Time-Invariant (LTI) systems with finite impulse response. An FIR filter is always stable and can have linear phase, whether the coefficient sequence in the filter is symmetric or antisymmetric. Its transfer function is a polynomial in z^{-1}, so it has only one pole at $z = 0$, inside the circle of unit radius. It is a non recursive moving-average filter, to compute the output you have to step-average the input numbers. The disadvantage of FIR filters is that in order to achieve the same performance as an IIR filter, larger orders must be used, and this results in longer transient durations so that the output samples will be affected by a longer delay than the input signal. The order of the filters applied determines the delay in samples;

- **IIR (Infinite Impulse Response)**: are systems with infinite impulse response. IIR filters have a non linear phase and are unstable. They are a recursive and autoregressive filters; some output values, in addition to input values, are required to generate the output, which are previously produced. The main disadvantage of IIR filters is due to the nonlinear phase, which introduces distortion into the signal that cannot be predicted a priori. Anti-causal (or double-pass) filtering must be applied to compensate for the distortion introduced by the filter. Compared with IIR filters they involve less computational complexity, less memory and fewer parameters.

EEG signals are commonly filtered by using a high-pass filter with a cut-off frequency ranging from 0.1 Hz to 1 Hz to remove slow drifts, and a low-pass filter is applied to eliminate frequencies above 40-50 Hz.
In this project, the signals were filtered with a high-pass filter with a cutoff frequency of 0.1 Hz and a low-pass filter with a cutoff frequency of 30 Hz. Both applied filters are of IIR type and were implemented utilizing the Matlab *butter* function.
Subsequently, the signal was resampled to a frequency of 256 Hz.

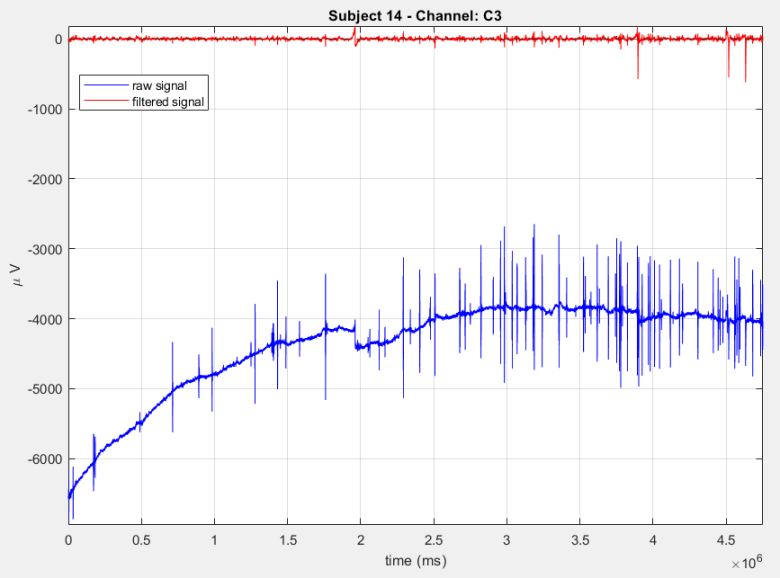

Figure 4.5: Subject 14: C3 channel signal before (blue) and after re-referencing and temporal filtering (red).

As can be seen in the [Figure 4.6], the spectral density of the signal after re-referencing and filtering has changed. Among the attenuated components is power line interference at 50 Hz.

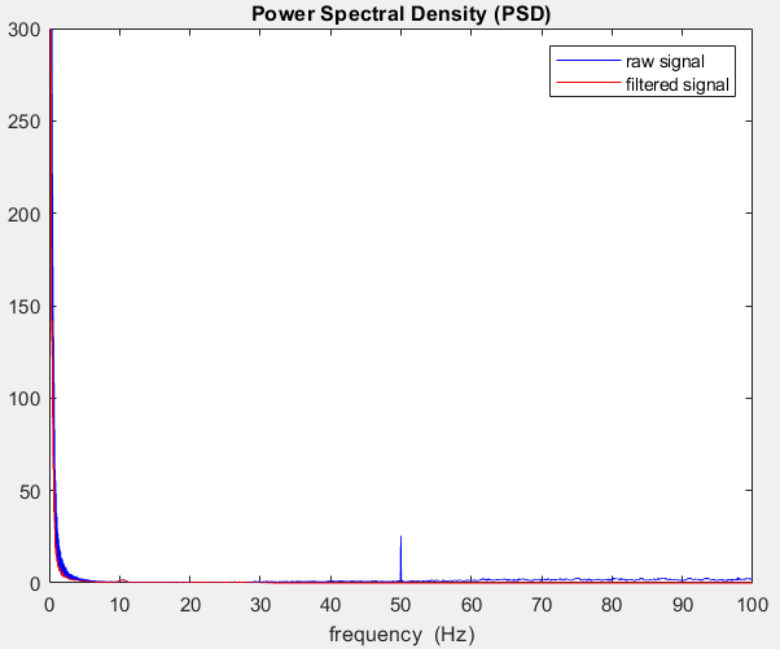

Figure 4.6: Subject 14: power spectral density (PSD) of the C3 channel signal before (blue) and after re-referencing and temporal filtering (red).

4.1.2 EEG Channels Operations and Artifact Correction

The next step is the identification and elimination of particularly noisy channels based on channel statistics. The *clean_artifacts.m* function provided by EEGLAB is used and specifically the noisy channels are determined by observing: flatline channels; bad channels based on probability, skewness and PSD; noisy channels according to correlation, line-noise thresholds, low-frequency drifts and short-time bursts. Once identified they are adjusted by calling the *pop_select.m* function provided by EEGLAB.

After removing the noise channels the subsequent step is the detection and correction of artefacts, which is done through *Independent Component Analysis* (ICA). ICA extracts a set of components and isolates artefacts through statistical properties. The algorithm used in SEPLab is the algorithm used in MRCPLab and adapted to these signals. Sejnowski and Bell, at Salk Institute in 1995, conducted the first decomposition of multi-channel EEG data into distinct components. They utilized the *infomax algorithm*, which operates on the principle that weighted combinations of independent source signals that can be separated into individual source signals without needing any prior information about the nature of these sources, in particular to separate signals exploits their buffer independence. The

example generally used to best understand this problem is the *cocktail party problem*. The problem considers multiple microphones at a party simultaneously capturing conversations of different people. Each recording taken individually sounds like incomprehensible 'party noise'. The challenge of blind source separation involves figuring out how to mix these recorded signals to isolate each speaker's voice, without any prior knowledge about the characteristics or properties of the individual sources. This helps the ICA, which is able to focus its attention on a single sound by separating them [40]. Consider the X matrix as the signal recorded on the scalp, the ICA searches the W matrix (unmixing matrix) to deconstruct the signal into independent U components, also referred to as IC activations.

$$U = WX \tag{4.2}$$

The mixing matrix, which is the inverse of the unmixing matrix ($W^{-}1^{1}$), reconstructs the scalp data by multiplying it with the IC activation matrix ($X = W^{-}1^{1}U$) [Figure 4.7].

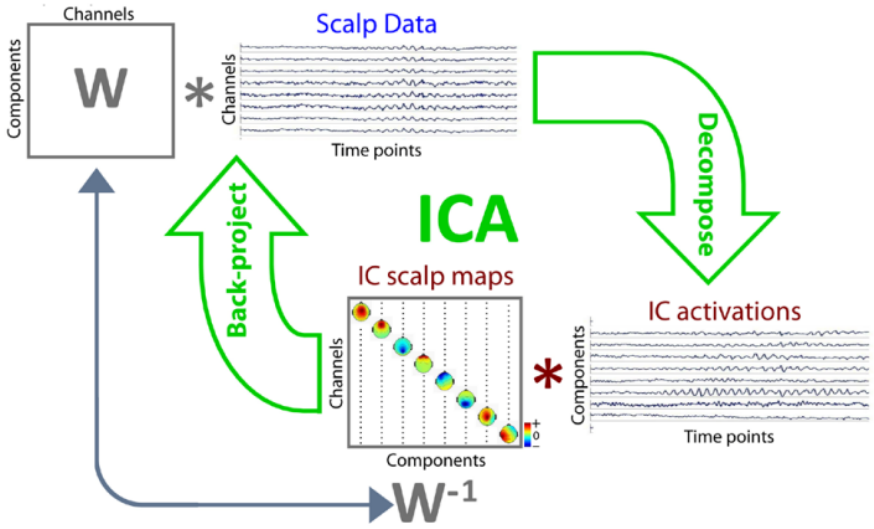

Figure 4.7: . Flowchart for ICA data decomposition and back-projection. Taken from [40]

This source separation method is appropriate for situations where the sources are independent, the mixing medium has negligible propagation delay, the analog sources have a probability distribution that is not exactly Gaussian, and the number of IC components matches the number of sensors. Of these hypotheses, the first two can be fulfilled by EEG signals, because the EEG dynamics can be represented as a set of statistically independent brain processes, with the volume

conduction occurring instantaneously. The third assumption is reasonable because EEG sources are typically sparsely active and therefore deviate significantly from a normal distribution. For the last hypothesis to be able to obtain a correct decomposition with ICA, it is ideal to use an adequate amount of data, as the actual number of statistically independent sources is not known [40][41].

The function used in the plug-in to identify independent components is *runica*. The function receives as input the signal, a matrix of nCh x t (where nCh is the number of channels and t is the time expressed in samples) returns as output the activation matrix nIC x t and the sphere matrix nCh x nCh, the matrix that eliminates the correlation between the components.

$$activation = weights \cdot spere \cdot EEGdata \tag{4.3}$$

Compared to MRCPLab, no EOG signals are available in this project, but the AF3 and AF4 channel signals were chosen to be used as such, in order to improve the identification of ocular artefacts.
The goal of the algorithm is to detect muscle and eye artefacts and focal components typical of noisy channels. Pearson's correlation coefficient allows the identification of ocular artefacts by providing a measure of the linear dependence between two variables A and B (Equation 4.4).

$$\rho(A,B) = \frac{cov(A,B)}{\sigma_{\mathrm{A}}\sigma_{\mathrm{B}}} \tag{4.4}$$

where cov(A,B) is the covariance of the variables A and B, σ_A and σ_B are the standard deviation. The linear dependence (ρ) is assessed for each component and for the signal of the AF3 and AF4 channels using Matlab's *corrcoeff* function. The IC with the highest ρ is identified as an artefact and corrected immediately. Other specific features in the time and frequency domain are evaluated for each IC [42].

- **Fit-error:** refers to the departure of a component's spectrum from a prototypical curve, its shape is defined as $\frac{1}{f}$, where

$$f \rightarrow \frac{k_1}{f_\lambda} - -k_2 \tag{4.5}$$

  The parameters k_1, k_2 and λ are strictly positive and defined by three log spectrum points: value at 2 Hz, the local minimum in two different bands [5-13] Hz and [33-39] Hz;

- **Average log band power:** the average logarithmic power is evaluated over the frequency range [8-13] Hz;

- **Focal component:** the measure is obtained by the greatest z-score of the mixing matrix W^{-1}:
$$F = max(Z(W^{-1})) \tag{4.6}$$

- **Kurtosis and Swkewness:** analysing and identifying cardiac and ocular artefacts. Both are statistical features of the signal.
Kurtosis assesses the pointedness of a distribution's peak and is determined as:
$$K = \frac{E(x-\mu)^4}{\sigma^4} - 3 \tag{4.7}$$
Skewness quantifies the symmetry of a probability distribution:
$$S = \frac{E(x-\mu)^3}{\sigma^3} \tag{4.8}$$

- **Entropy:** is a statistical measure of causality and it is estimated as:
$$H = -\sum p(x) log_2(p(x)) \tag{4.9}$$
where p(x) represents the probability of seeing the activity levels of x in the distribution. Large entropy values are associated with values with low probability, conversely low entropy is associated with values with high probability.

A normalisation through the truncated mean standardising a variable without taking 0.1 per cent into account is used for entropy, kurtosis and skewness. Instead, a threshold of 1.5 is set for focal components. Finally, an expectation-maximisation algorithm is used to statistically evaluate the thresholds for the fit-error and mean logarithmic power.
After identifying artefactual components, they are corrected by setting them to 0. By multiplying the IC with the mixing matrix during EEG signal reconstruction, artifacts are minimized and have no impact on the final outcome [42].

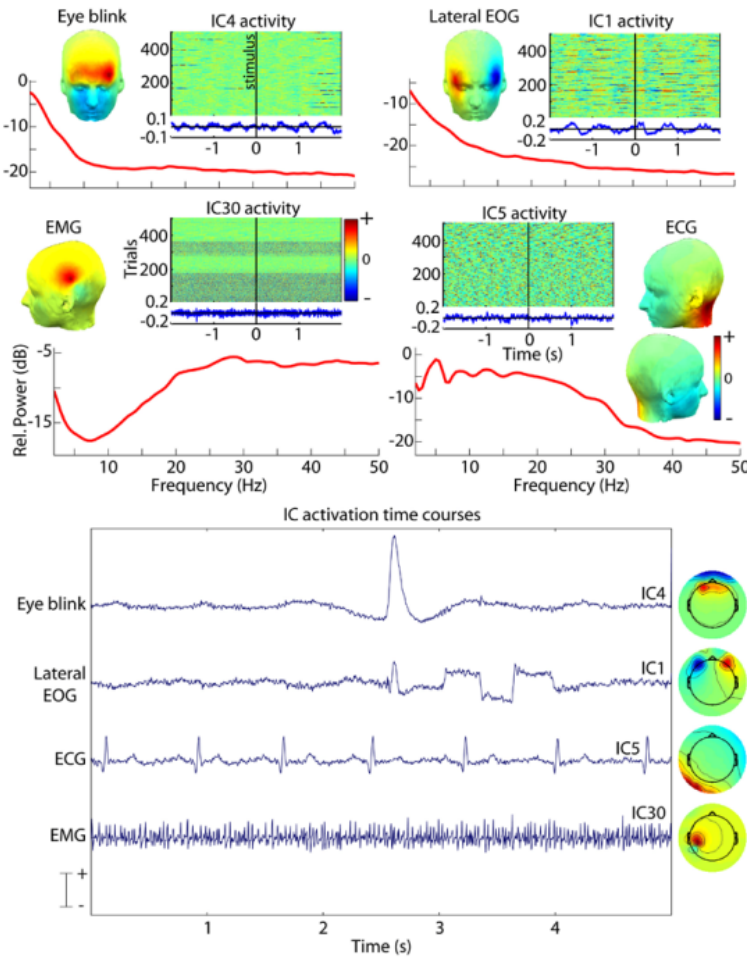

Figure 4.8: Illustration of possible independent components for eye blinks, lateral eyr movemnts, EMG and ECG activity respectively. Taken from [40]

Below are the results of the palm-up condition with and without applying artifact correction.

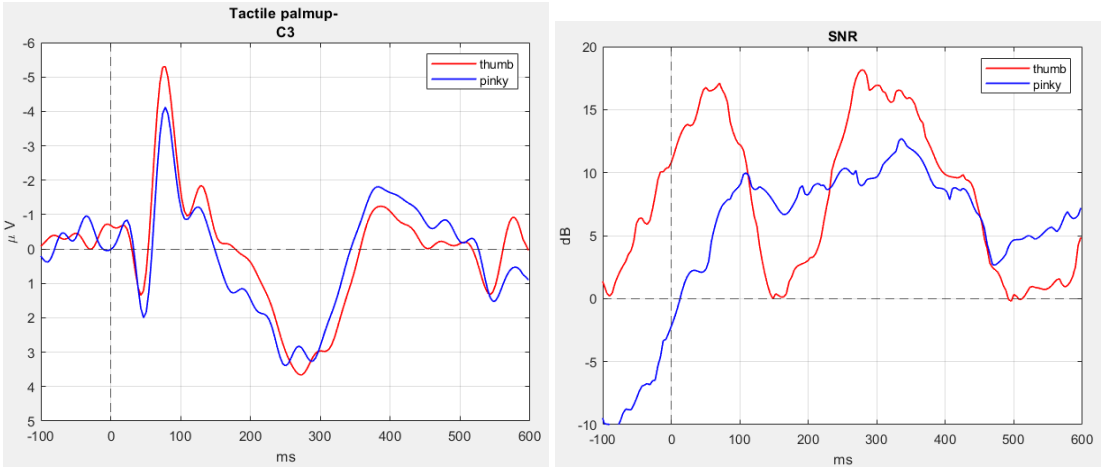

Figure 4.9: SEP and SNR (thumb in red and pinky in blue) obtained by re-referencing, temporal filtering, robust detrending and baseline correction methods.

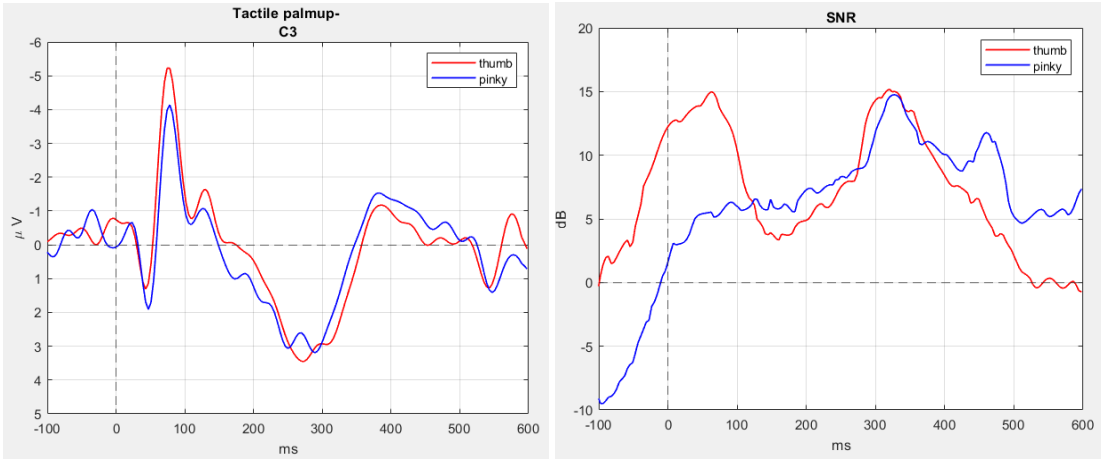

Figure 4.10: SEP and SNR (thumb in red and pinky in blue) obtained by re-referencing, temporal filtering, artefact correction algorithm, robust detrending and baseline correction methods.

After the correction of the EEG signal, the previously eliminated channels are added back in by interpolating the other channels (EEGLAB's *pop_interpolation_mrcp.m* function is used). The interpolation method used is the *spherical spline*. At the end of the process, the dataset will contain the original number of electrodes.

4.1.3 Epoch operation

The function (*pop_detrendandepoching.m*) has been implemented to perform the next step. It allows detrending, to divide the signal into epochs and to do baseline correction. These are described in detail below there.

Detrending

The EEG signal is affected by slow drifts, skin potentials or by the slight movement of the electrodes, which cannot be removed by linear combination as is the case of ICA, indeed their effects may be emphasised. Cortical activity in the low frequency range can be masked by the slow drifts, furthermore, when the data are epoched the drifts can be interpreted as a reproducible pattern in the trials. Methods that can be used to eliminate slow drifts are high-pass filtering or detrending [39].

The cut-off frequency used in the **high-pass filter** to eliminate slow drifts is between 0.1 and 2 Hz. In addition to the elimination of slow drift, slow cortical activities, both stimulus-evoked and spontaneous are also eliminated and the transient characteristics can be modified. The transient fluctuations due to the filter take time to smooth out and can be confused with a reproducible neural response in the case of an epoch-division signal. The high-pass filter can distort the signal and cause it to be misinterpreted, consequently other methods are used.

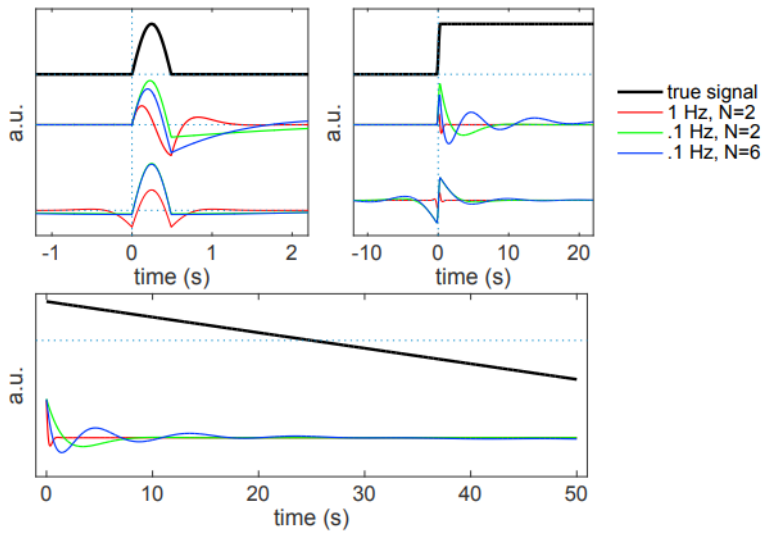

Figure 4.11: The top left figure shows the influence of the high-pass filter (Butterworth) as the order changes on a unipolar pulse of 0.5 s duration. As the filter type, order and cutoff frequency change, the signal is not only attenuated, but also distorted. The figure above right shows how the same filters affect a step with a rise time of 0.5 s, as might happen in the cerebral reaction to the onset of a stimuli. The bottom row of the figures above represents the response of the zero-phase filters. Instead, the image below depicts the reaction of the high-pass filter to a descending ramp. Taken from [39]

Detrending involves evaluating a smooth function f(t), typically a low-order polynomial, to best suit the signal x(t) and subtract it from the data:

$$y(t) = x(t) - f(t) \tag{4.10}$$

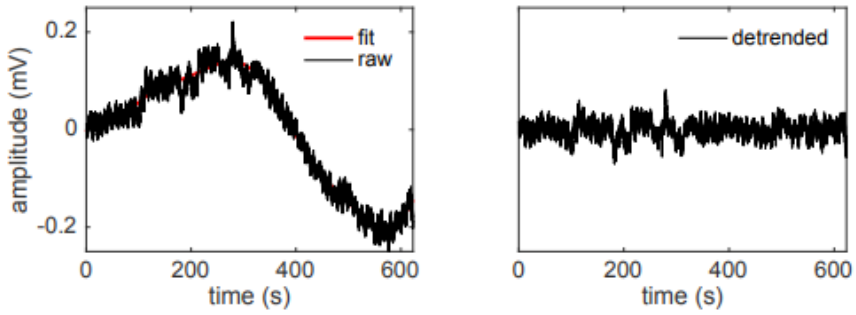

Figure 4.12: Detrending application.
Left: EEG signal affected by slow drift (black) and its 10-th order fitting line (red).
Right: EEG signal after removal of the fit. Taken from [39]

The scale of the fluctuations that are removed is governed by the order of the polynomial. Detrending is sensitive to temporally localised glitches, disturbances caused by lead or electrode movement, muscle artefacts.

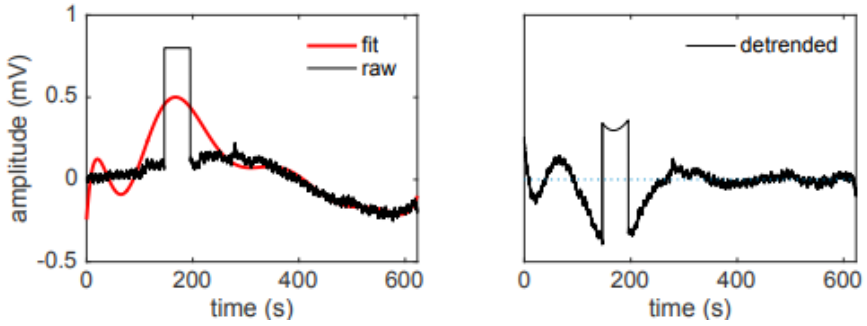

Figure 4.13: Detrending application in presence of a glitch.
Left: EEG signal with an artificial glitch inserted (black) and the polynomial fit (red). Compared to the previous case on the detrend signal high amplitude fluctuations are present over a range extending outside the glitch-contaminated part.
Right: EEG signal after removal of the fit. Taken from [39]

Robust detrending aims to reduce the impact of glitches on signal fit. The slow trend, which is removed, is approximated using a weighting matrix w(t). The weighted least squares approach is used to choose the best fitting line. Weights can be provided as a matrix or to inferred using a threshold [39].

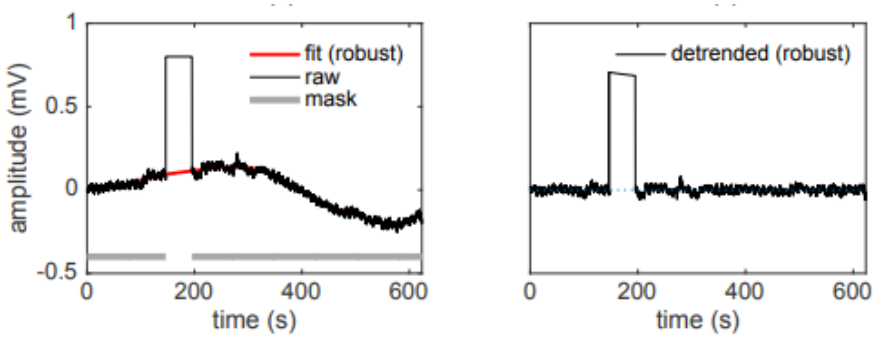

Figure 4.14: Robust Detrending application in presence of a glitch.
Left: EEG signal with an artificial glitch inserted (black) and the polynomial fit (red).
Right: EEG signal after removal of the fit. Respect to [Figure 4.13] shows that the fitting line does not account for glitches, and subtraction does not cause deformations. The grey line shows a weights matrix of zero for glitch duration. Taken from [39]

Due to the weak nature of ERPs, it is not certain that robust detrending identifies and masks cognitive events of interest. This may adversely affect the quality of the data, as a partial fit to an ERP peak may result in erroneous and inverted patterns of activity with respect to the baseline or due to the polynomial fit to the real and non-weak ERPs, so removing it from the signal eliminates the real and non-weak effects [43].

Algorithm 1 Robust detrending algorithm

Require: EEG signal x(t)
Ensure: detrended EEG y(t), outlier map w(t)
    Initialize w(t) ← 1
    while not finished **do**
        f(t) ← x(t) fit to basis functions using weights w(t)
        d(t) ← |x(t)-f(t)|
        if |d(t)/STD(|d(t)|)> threshold **then**
        else
            w(t) ← 1
        end if
    end while

In the plug-in, the robust detrending described in (1) was applied via the function of Noise Tools toolbox *nt_detrend* and the order was set to 4 after several attempts.

The signal was split up in order to get a better result as the complete signal is very long. As input to the nt_detrend function, in addition to the order, a part of the signal with a length of 434 samples (1.7 s) is provided.

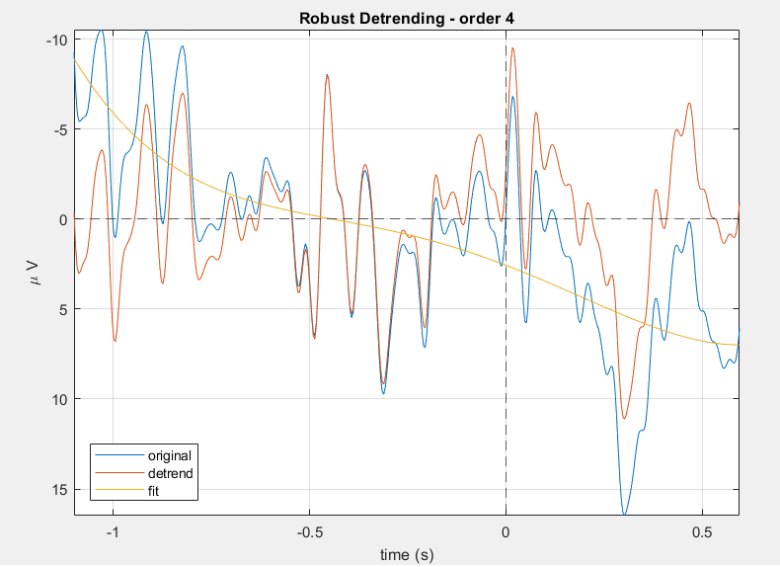

Figure 4.15: Robust Detrending on a portion of the signal along 434 samples of channel C3

Epoching and Baseline Correction

Subsequently, the signal is epoched in epochs of 256 sample lengths (in time has a duration of 1s). Specifically starting from the stimulus which is pointed to zero and considering 400 ms before and 600 ms after the stimulus. After epoching, baseline correction is performed using a 400 ms window preceding the stimulus onset. For each channel, the average activity calculated in the chosen window is subtracted in order to eliminate the spreading effects of DC offset suppression, which can introduce spurious effects into the prestimulus and immediate poststimulus intervals. It is assumed that no relevant experimental information is contained in the chosen window [43].

4.1.4 Jitter compensation

Trial-to-trial latency variability

To obtain SEPs, it is essential to average a sufficiently large number of single-trial EEG responses, assuming that the key components elicited by a stimulus are time-locked to the stimulus onset, and that the variations between trials are just noise

[Figure 4.18(A)]. One of the problems with averaging epochs is the **variability of latency from trial-to-trial**, obscuring SEP-averaged waveforms, decreasing their amplitude and hiding the physiological importance of the consequences of a particular condition [Figure 4.18(B)].

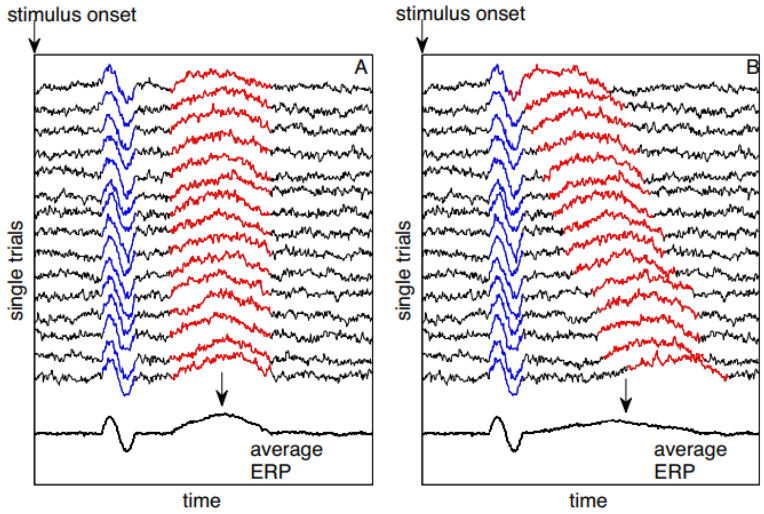

Figure 4.16: Illustration of individual ERP trials.
A) All ERP components are time-locked to the onset of the stimulus.
B) Some ERP components are not temporally synchronized upon stimulus onset.Taken from [44]

Numerous studies have shown that ERP components exhibit significant variability in latency across different trials, leading to a smearing effect that reduces the amplitude of the averaged ERP. The consequences due to the variability of latency between different trials may be as follows [Figure 4.17]:

- *Same latency variability from trial to trial but different amplitude:* it may be difficult to distinguish the amplitude differences between conditions. As the amplitudes are reduced, the background noise could be of a similar magnitude to the actual signal, hindering the accurate detection and identification of the potential and affecting its statistical parameters;

- *Same amplitude but different trial-to-trial latency variability:* differing degrees of amplitude attenuation may arise, creating an artificial amplitude difference between conditions. Such discrepancies may be mistakenly attributed to differences in the intensity of the activity of the underlying neural system rather than to different levels of temporal variability in brain activities in individual trials.

Distortion of the single epoch ERP due to latency variability in the average waveform can lead to inaccurate results. As shown in the [Figure 4.17], in the first case the amplitude difference is reduced, while in the second case it indicates the presence of an amplitude difference even if it is not present [45].

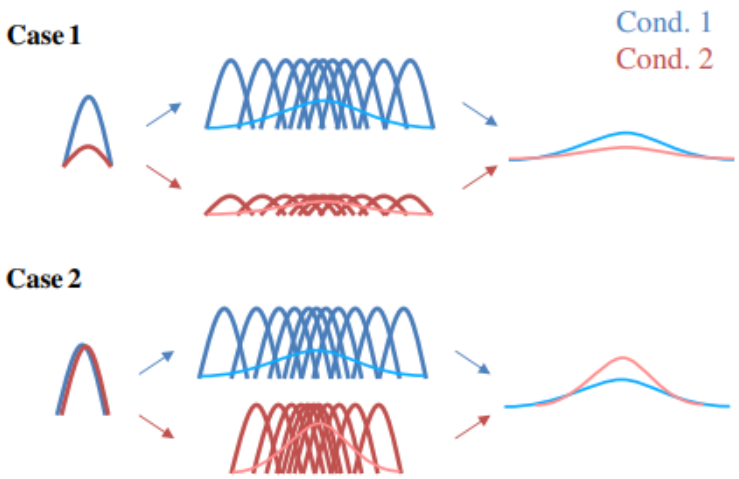

Figure 4.17: Smearing effect due to trial-to-trial latency variability. ERP components for two conditions are represented by blue and red sinus half-waves, respectively.
Case 1: The amplitude difference in the averaged ERPs for the two conditions with the same latency variability is reduced due to trial-to-trial latency variability.
Case 2: An apparent difference in amplitude between the averages of the conditions is created by the different variability of the latency from process to process present in the two components with the same amplitude. Taken from [45]

Jitter Compensation: Woody's method

The most widely used method for dealing with latency variability is Woody's method first proposed in 1967. It is an iterative method that uses correlation to estimate latency variability. The procedure can be summarized as follows [46]. In the signal model, $x_i(n)$ denotes the amplitude of the ith observation at the time sample $n(0 < n < \mathrm{N})$, $i = 1,..\mathrm{I}$, the total number of trials. Each epochs consists of an unknown transient template wave $s(n)$ delayed by d_i, expressed as $s_{di}(n) = s(n\text{-}d_i)$, plus $\mathbf{e}_i(\mathrm{n})$ epoch's noise.

$$x_{\mathrm{i}}(n) = s_{\mathrm{d_i}}(n) + e_{\mathrm{i}}(n) \tag{4.11}$$

The objective is to estimate the delay d_i from noisy observation that results from averaging data signals and iterative correlation. The delay d_i for the ith trial is estimated from an initial estimate of the model and epochs (Equation 4.12).

$$\hat{d}_{\mathrm{i}} = \arg\max \mathrm{d}_i \frac{1}{N} \sum_{n=1}^{N} x_{\mathrm{i}}(n) \hat{s}_{\mathrm{d}_i}(n) \tag{4.12}$$

N represents the number of data samples for each trial.
The average of all trials provides the initial model estimate. At each iteration i, the cross-correlation between the model and the ith trial is calculated, and its maximum indicates the lag $\hat{d}_i$. Each ith trial is corrected by its lag $\hat{d}_i$ after estimating it for all, and the new template is determined from the average of all trials. Then the new delays ($\hat{d}_i$) are computed in the new iteration on i ranging from 1 to I until convergence. A limitation of Woody's method is that it allows variability only in latency and not in amplitude, which the method of Jaskowski and Verleger [46].

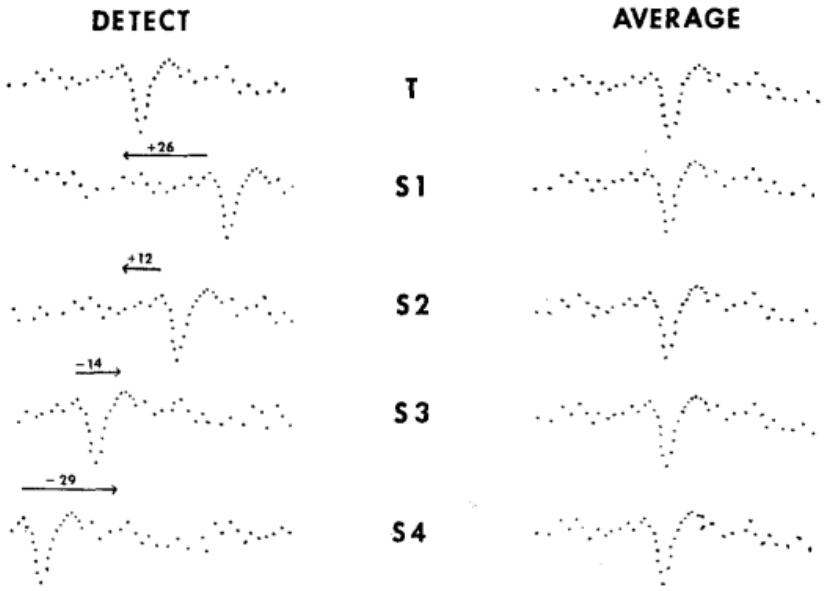

Figure 4.18: Woody Method: The trials (S1-S4) were shifted by a certain lag calculated through the cross-correlation between individual trials and the template (T). Trials are averaged after being realigned. Taken from [47].

Jitter Compensation: Matlab function

The algorithm implemented in the Matlab function (*pop_jitter_compensation.m*) relies on the correlation among epochs, specifically utilizing Pearson's linear correlation. This method is advantageous due to its simplicity and computational efficiency, but it is limited to detecting only linear relationships, so, it is assumed that brain activity operates as a linear system, which is a reasonable approximation. Therefore, we compute all possible correlations over time using the cross-correlation function. The cross-correlation function assesses the correlation between two signals by keeping the first signal fixed in time and shifting the second signal temporally, forward or backward.
The following describes the jitter compensation, step by step,that has been implemented in SEPLab.

1. The beginning template is defined by mediating all epochs. The cross-correlation between the template and epochs is calculated to find the first epoch best correlated with the template. The epoch with the highest correlation value, which are saved in a vector, is selected. The vector does not contain the maximum cross-correlation values of each epoch, but the value selected by applying a threshold. The threshold chosen is 50% of the maximum value of the cross-correlation, it varies between epochs. The peaks that have a value greater than this threshold are identified and the one to which the least lag corresponds is selected;

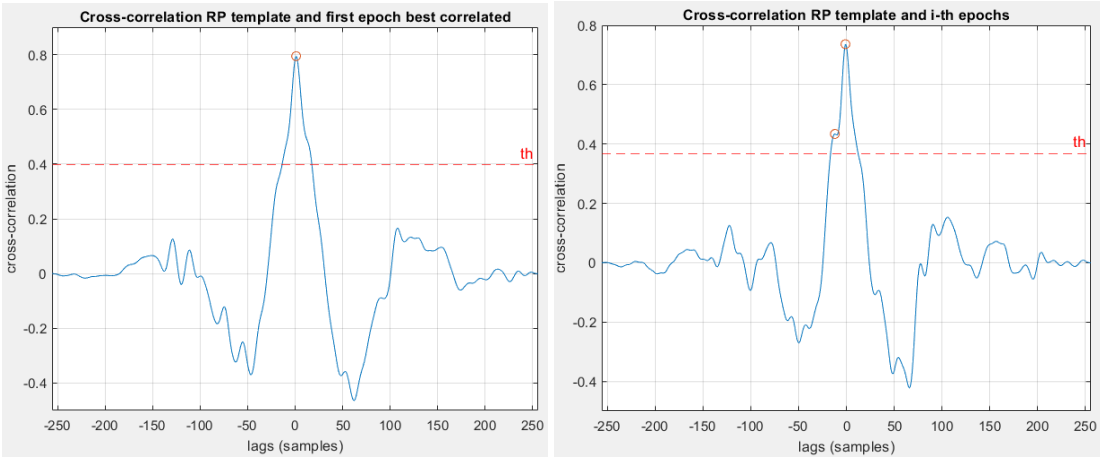

Figure 4.19: Illustration of the cross-correlation for jitter compensation of subject 14.
The left figure shows the correlation of the first template (average of all epochs) with the first best-correlated epoch.
The figure on the right shows the correlation of the first template with a generic epoch. As can be seen in this case, two peaks greater than the threshold have been identified, but the delay selected is the minimum between the two (in the case in the figure it is 0).

2. The best related epoch selected is the new template. The cross-correlation between the first best-correlated epoch and all remaining epochs is calculated. The same process used before is repeated to find the second best-correlated epoch to the first;

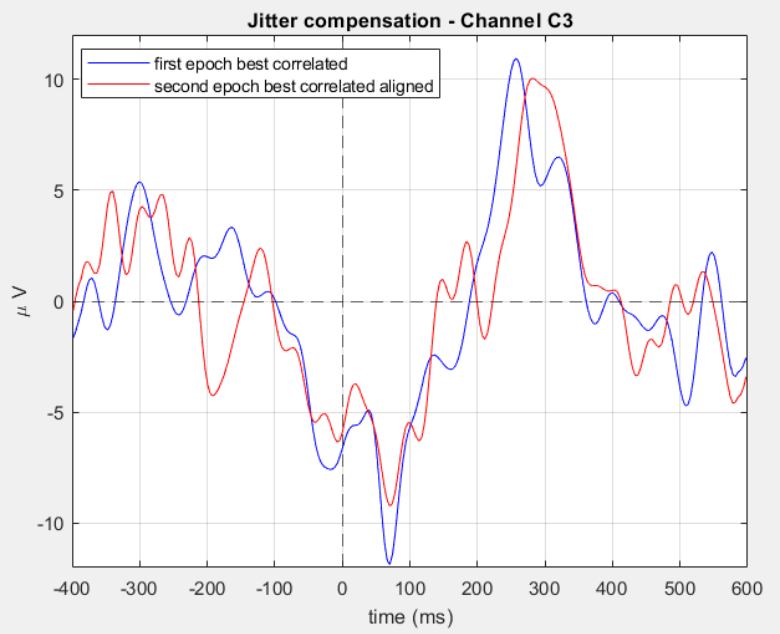

Figure 4.20: Plot of the first best-correlated epoch and the second best-correlated epoch after realignment. In the next step the two epochs will be averaged to create the new template.

3. The second best correlated epoch is shifted relative to the first best correlated epoch of the previously identified delay. It is assessed whether the alignment was performed correctly by calculating the cross-correlation between the first two best-correlated epochs. It is checked if the maximum of the correlation function does not differ much from the zero value, because after the alignment the maximum must be in zero. The epoch is discarded if the difference is greater than 10%. The user can vary the value by 10%. This evaluation is done because the cross-correlation after alignment must have a maximum in zero, but there may be cases where the cross-correlation function may increase toward one of the two epoch extremes (left or right). This *edge effect* could lead to a value where the correlation is even higher but with a non-zero lag. This correlation is spurious and most likely caused by artefacts, so these epochs must be removed. However, one can have signals in which the edge effect, even if it is present is not particularly significant;

4. The value of the template is recalculated by averaging the first best-correlated

epoch and the second best-correlated epoch aligned, if it has not been excluded. Otherwise, the new template will consist of only the first best correlated epoch;

5. Then the new epoch best correlated to the new template is calculated. The correlation between the new template and the remaining epochs is calculated and the one with the highest correlation is selected, calculated as described in the previous points via the threshold. Before proceeding with the alignment, the validity of the epoch is assessed by checking if the value of the cross-correlation is less than a certain factor. In that case the epoch will be discarded otherwise it will be realigned to the template. The factor is defined as the difference of the median value, calculated on the matrix that contains the correlations of each epoch after the calculation of the cross-correlation between the first template (average of all epochs) and each epoch, and the product of the standard deviation calculated on the same matrix and the multiplicative value 1.5 (value that can be modified by the user). Then the alignment is checked if the epoch has not been excluded and evaluated as described above in point 3;

6. The new template is recalculated by averaging the aligned signals (first best correlated epoch, second best correlated aligned epoch, third best correlated aligned epoch). If the third best correlated epoch is excluded, the template will be the same as the previous one;

7. We repeat steps 5 and 6, recalculating the cross-correlation between the template and the remaining epochs, until we iterate over all the epochs;

8. Finally, all epochs of all channels are realigned with respect to the C3 channel.

The latency jitter compensation is not computed separately for each channel. Instead, the shift applied to align each epoch to the one with the highest correlation is determined based on the epochs of channel C3, which serves as the reference. This same shift is then uniformly applied to the corresponding epochs of all other channels. As a result, the temporal evolution of the event-related potential, which is not uniformly distributed across the cortex, is not accurately represented. Different channels may exhibit varying delays due to their differing distances from the origin of the potential, resulting in signals reaching the electrodes at different times.

4.1.5 SEP operation

In the case of event-related potentials, the component of interest is superimposed on the unwanted signal, represented by the background EEG, which is assimilated as noise. In this context, the signal-to-noise ratio (SNR) is low due to the higher amplitude of the EEG signal compared to the SEP and the superimposed frequency

content. To overcome this problem and to be able to identify the components of interest in the SEP, *time-domain averaging* is used and trials are averaged. In this way, the noise being a stochastic is reduced by a factor of $1/\sqrt{N}$ (N number of trials), while the constant and synchronised components add up in phase.

$$x_{\mathrm{m}}(t) = \frac{1}{N}\sum_{i=1}^{N} x_{\mathrm{i}}(t) = \frac{1}{N}\sum_{i=1}^{N}(s_{\mathrm{i}}(t) + e_{\mathrm{i}}(t)) = s(t) + \frac{1}{N}\sum_{i=1}^{N} e_{\mathrm{i}}(t) \tag{4.13}$$

where $\mathrm{x}_i(\mathrm{t})$ is the related event contained in the i-th trial, s(t) is the deterministic ERP equal in all trials, $\mathrm{e}_i(\mathrm{t})$ is the zero mean value noise superimposed on the ERP of interest.

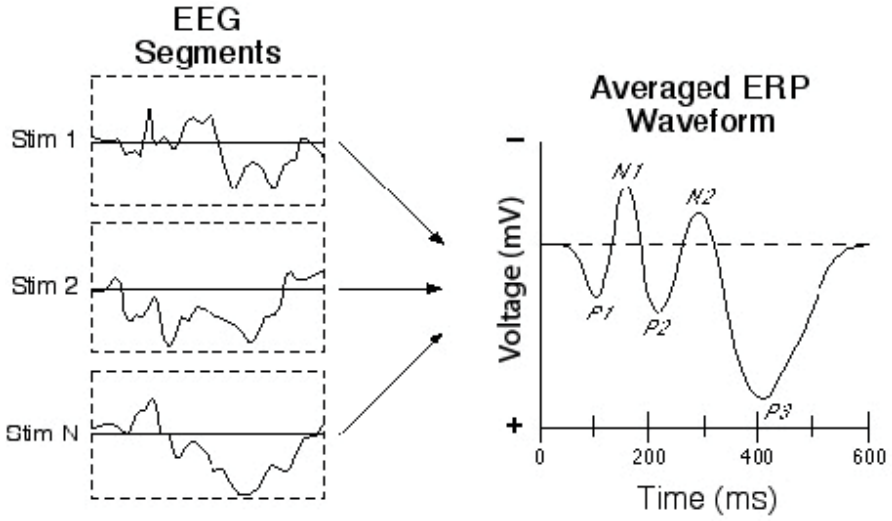

Figure 4.21: Illustration of the averaging on three trials. Taken from [48]

4.1.6 Plot and SNR

The SNR is calculated by making the difference between the SEP calculated by averaging the odd epochs (SEP_1) minus the SEP calculated by averaging the even epochs (SEP_2). The SEP, as described above, consists of two components: signal and noise. If we considers SEP_1 and SEP_2 as the sum of the signal plus the noise, what differentiates them is precisely the noise. If the difference of the two estimates is made, the signal s(t) is cancelled as it is deterministic, whereas the noise e(t) remains because it is additive since being a stochastic process (Equation 4.14).

$$\begin{aligned} SEP_1(t) &= s(t) + e(t)_1 \\ SEP_2(t) &= s(t) + e(t)_2 \\ SEP_1(t) - SEP_2(t) &= s(t) + e(t)_1 - [s(t) + e(t)_2] = e(t)_1 - e(t)_2 \end{aligned} \tag{4.14}$$

Below there are the results of one test subject, distinguished according to palm orientation. The *movmean* function, a moving average filter, was applied in the signal plot.

The first results shown concerns touching the thumb and little finger with the palm of the hand facing down.

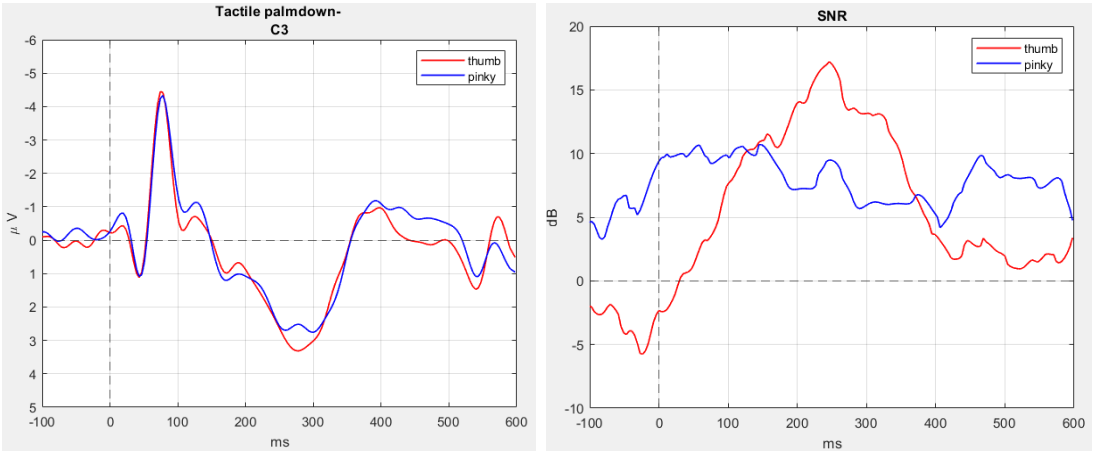

Figure 4.22: Palm-down condition: SEP and SNR (thumb in red and pinky in blue) obtained by re-referencing, temporal filtering, artefact correction algorithm, robust detrending and baseline correction methods.

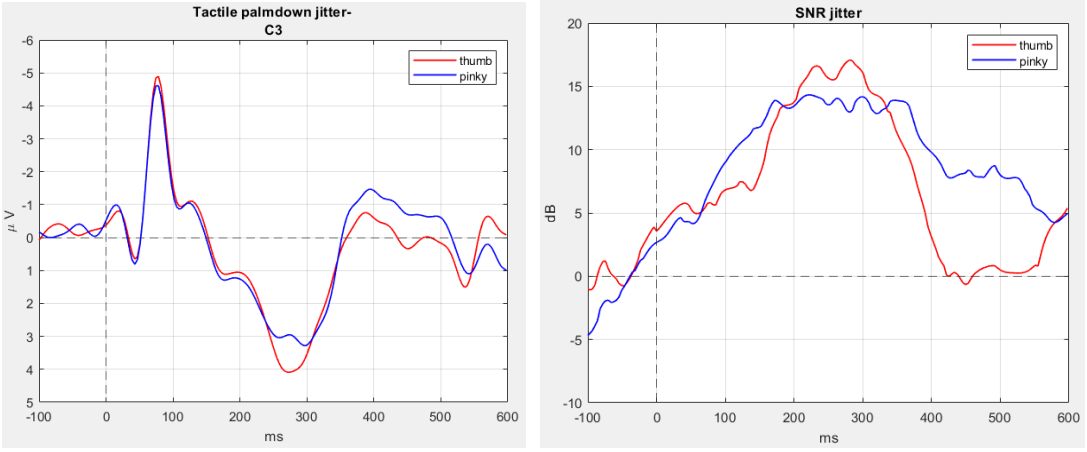

Figure 4.23: Palm-down condition: SEP and SNR (thumb in red and pinky in blue) obtained by re-referencing, temporal filtering, artefact correction algorithm, robust detrending, baseline correction and jitter compensation

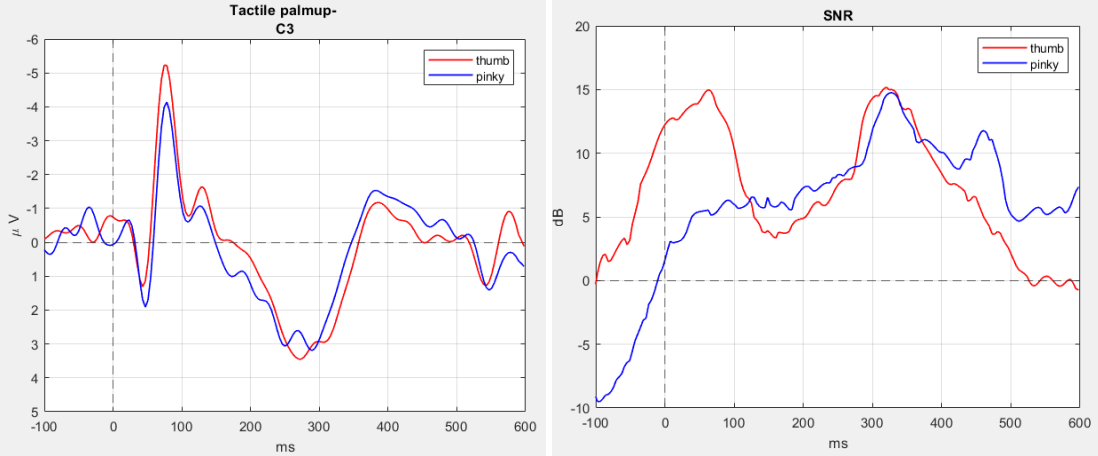

Figure 4.24: Palm-up condition: SEP and SNR (thumb in red and pinky in blue) obtained by re-referencing, temporal filtering, artefact correction algorithm, robust detrending and baseline correction methods.

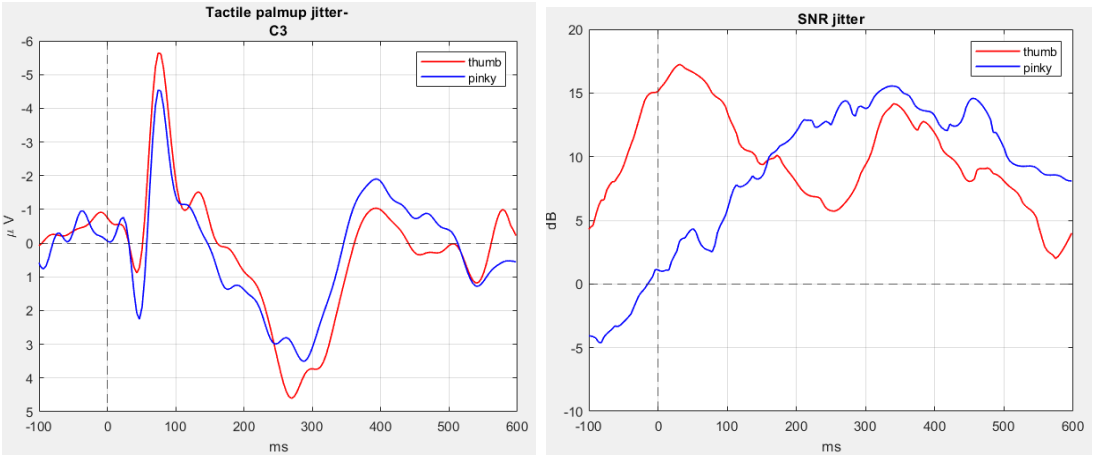

Figure 4.25: Palm-up condition: SEP and SNR (thumb in red and pinky in blue) obtained by re-referencing, temporal filtering, artefact correction algorithm, robust detrending, baseline correction and jitter compensation.

From the results, it can be observed that after the application of jitter compensation, the N80 and P300 components increased in amplitude, particularly for the thumb case. It can be observed in the [Figure 4.23] that the SNR of the pinky palm-down case after the application of jitter compensation improves, particularly in the time window [200 400] ms. An increase in SNR can also be observed in the palm-up case. Therefore, the implemented pre-processing chain allows the characteristic components of the SEP to be enhanced and the SNR to be improved.

Chapter 5

Results

5.1 Grand Averaging

In the study of somatosensory signals, different subjects are mediated to each other. This is done with the aim of identifying stable components, therefore by averaging the subjects, irrelevant variations are eliminated and signal components that are common between all subjects emerge more clearly. This enhances the signal of interest and reduces noise, because SEPs are generally very weak compared to the background noise present in the electrical activity of the brain. In addition, there is variability between subjects in terms of electrophysiological characteristics, physiology and anatomy; by averaging them, the representative signal is obtained as the influence of individual variations is reduced. Furthermore averaging a larger sample the validity and statistical power of the results increase, making the data analysis more robust and allowing more reliable conclusions to be drawn. Below there are the results of averaging the subjects of the four conditions with the corresponding SNRs.

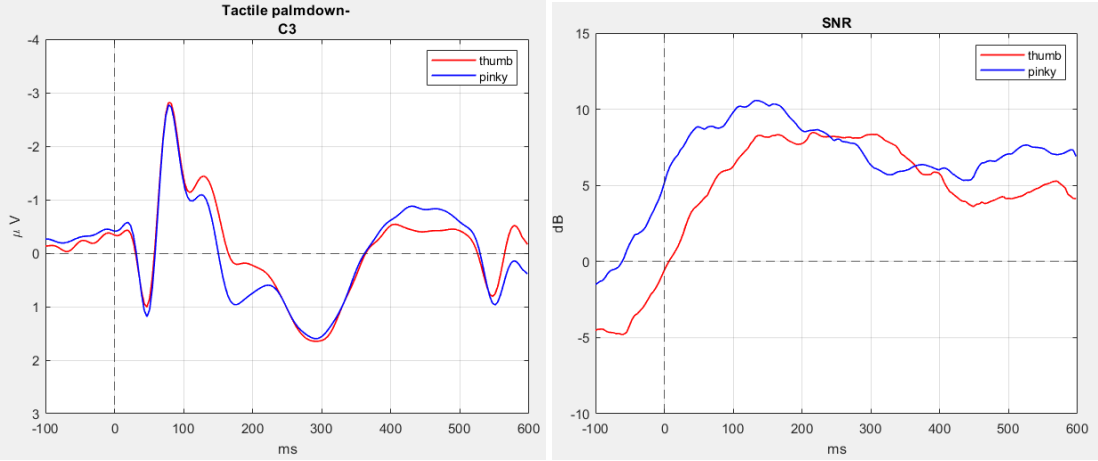

Figure 5.1: Palm-down condition: SEPs and SNRs of the average between subjects (thumb in red and pinky in blue) obtained by re-referencing, temporal filtering, artefact correction algorithm, robust detrending and baseline correction methods.

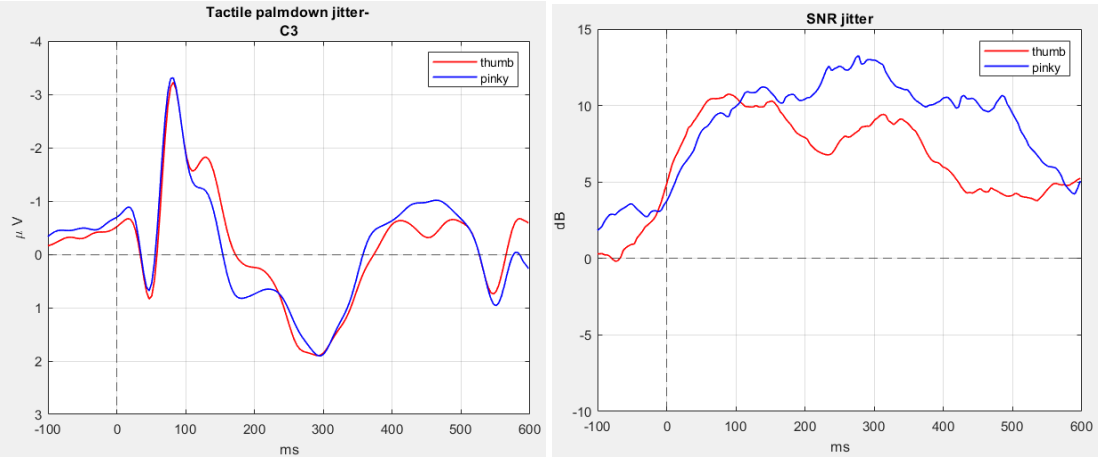

Figure 5.2: Palm-down condition: SEPs and SNRs of the average between subjects (thumb in red and pinky in blue) obtained by re-referencing, temporal filtering, artefact correction algorithm, robust detrending, baseline correction and jitter compensation

The Figure 5.1 and Figure 5.2 illustrate the SEPs and SNRs obtained by averaging 13 subjects for thumb and little finger in the palm-down condition. The SEPs and SNRs shown in the Figure 5.1 were obtained by averaging the subjects processed by applying the following pre-processing chain: re-referencing, temporal filtering, artifact correction, robust detrending and baseline correction. For the SEPs and SNRs in the Figure 5.2, however, a further step was added to the pre-processing

chain: jitter compensation. As can be seen in both cases, the SEPs present the following peaks: P45, N80, N140 and P300. In the second case under consideration, a greater amplitude of the wave can be observed, with a latency of about 300 ms. In addition, the jitter compensation algorithm leads to an improvement in the signal-to-noise ratio as can be seen in the Figure 5.2. In the case of the touch on the thumb there is a greater increase in the SNR for the early potentials (P45), specifically the SNR takes on a value of 9.5 dB compared to an initial value of 3.6 dB in the case without having applied jitter compensation. Whereas in the case of the little finger, a greater increase is observed for the SNR of the late potentials (the P300), the SNR goes from a value of 6 dB to a value of approximately double that (12.9 dB). Therefore jitter compensation helps to improve the signal-to-noise ratio.

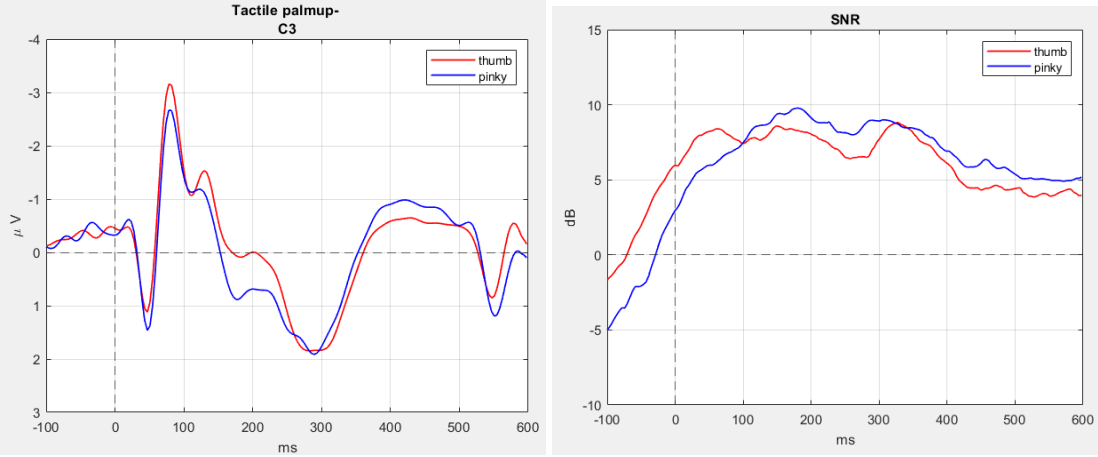

Figure 5.3: Palm-up condition: SEPs and SNRs of the average between subjects (thumb in red and pinky in blue) obtained by re-referencing, temporal filtering, artefact correction algorithm, robust detrending and baseline correction methods.

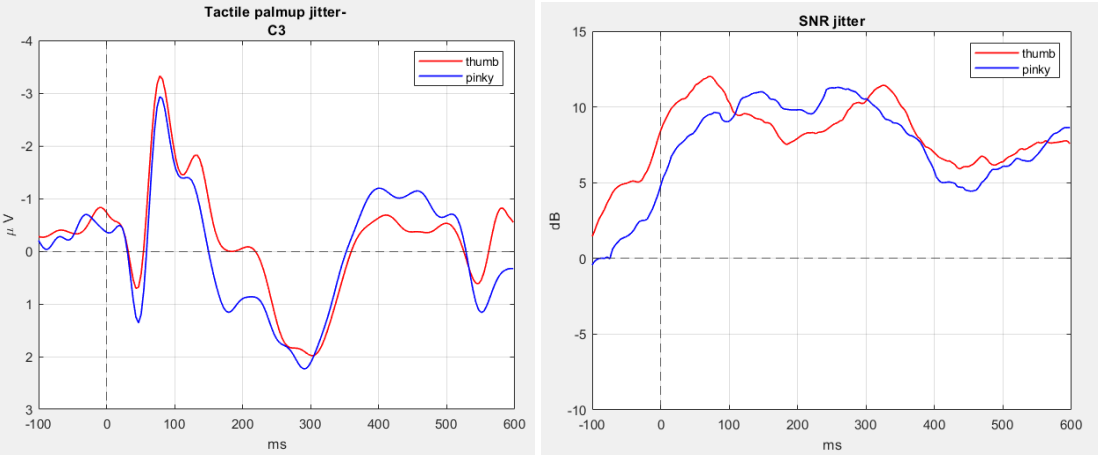

Figure 5.4: Palm-up condition: SEPs and SNRs of the average between subjects (thumb in red and pinky in blue) obtained by re-referencing, temporal filtering, artefact correction algorithm, robust detrending, baseline correction and jitter compensation

The Figure 5.3 and Figure 5.4 illustrate the SEPs and SNRs obtained for the palm-up condition. For this condition, as well as for the previous one, the following peaks P45, N80, N140 and P300 are present in the SEPs. In addition, in the same condition, the application of the jitter compensation algorithm leads to an improvement of the signal-to-noise ratio.

In this thesis project, brain activity recorded by the C3 channel was observed. The C3 channel is positioned on the hemisphere contralateral to the stimulated side and detects activity at the level of the primary somatosensory cortex. Regardless of the orientation of the palm and the finger on which the touch occurred, the presence of determined peaks can be observed:

- *P45:* is generated mainly in the primary somatosensory cortical area and is an early component. Upon finger touch, tactile receptors transmit the electrical signal through afferent nerve fibers. P45 is indicative of the time when the brain recognizes and begins to consciously process the tactile stimulus, as it reflects the synaptic activity and processing of tactile information occurring in the S1. In the results shown above, P45 occurs with a latency of about 31-35 ms, depending on the palm-up or palm-down condition. In all conditions it reaches the maximum peak at 46 ms after stimulus onset. It has an amplitude of approximately 1 µV in the palm-up and palm-down condition for the pinky and for the thumb palm-down condition and is less than 1 µV for the thumb palm-up condition;

- *N80:* is generated mainly in area S1 and is a medium latency component. It is a negative deflection found on the middle and posterior electrodes, which are areas involved in higher level sensory processing. In the results, the N80 component peaks at a latency of 78 to 82 ms after the stimulus;

- *N140:* is generated in the secondary somatosensory cortex and modulates attention. It is a wave with negative deflection and is a late latency component. Observing the results obtained, it can be seen that the N140 component is more pronounced in the case of touch on the thumb than touch on the little finger. It reaches its maximum peak at $\sim$ 128 ms in the palm-down condition and at $\sim$ 132 ms in the palm-up condition. It has a smaller amplitude than the N80 component;

- *P300:* is a wave with positive deflection and originates in the higher cortical areas (including the parietal cortex and other associative areas of the brain). This component reflects cognitive processes such as attention and conscious awareness of the stimulus. In the results it has an amplitude of about 2 µV and the positive deflection begins at $\sim$ 210 ms and peaks at $\sim$ 290 ms.

In the figures below, the topographies at 45 ms, 80 ms, 130 ms and 300 ms are shown alongside the SEPs. It can be seen that in the four conditions the results mirror those expected, in terms of latency and brain activation. In the case of the P45 component, it can be observed through the topographies that, in all the conditions studied, at 45 ms after the start of the stimulus the brain activity is concentrated more around the C3 channel which, as previously mentioned, registers

activity at the level of the primary motor cortex and it is the indicative time when the brain begins to consciously process the tactile stimulus. Also in the results of the topographies at 130 ms and 300 ms. In the first case the activity is concentrated in the associative cortical areas of the parietal lobe; while, for the P300 component the greatest activity is recorded in the frontal and parietal areas and it reflects conscious awareness of the stimulus. In the case of the N80 component, it can be seen that the greatest activity is recorded in the region ipsilateral to the stimulus and is recorded by the middle and posterior electrodes.

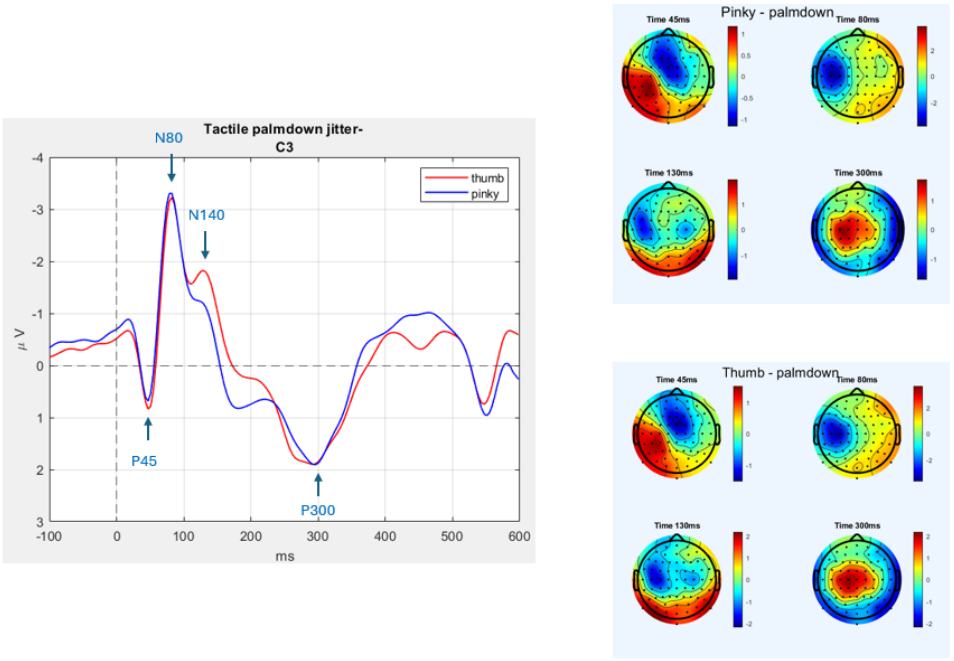

Figure 5.5: Illustration of the SEPs in the palm-down condition and the relative topographies at 45 ms, 80 ms, 130 ms 300 ms after the stimulus onset.

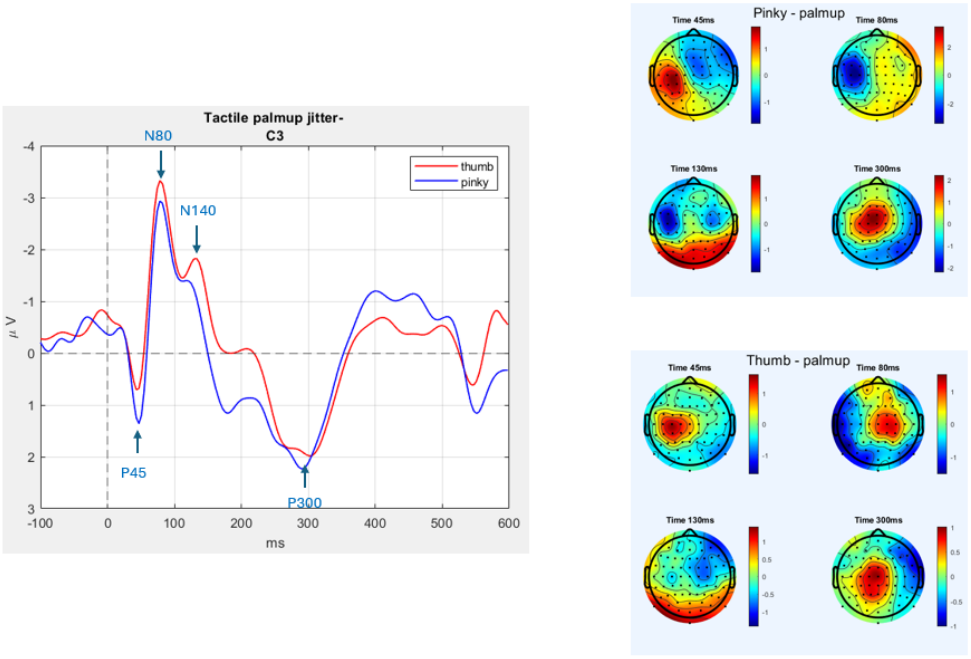

Figure 5.6: Illustration of the SEPs in the palm-up condition and the relative topographies at 45 ms, 80 ms, 130 ms 300 ms after the stimulus onset.

.

5.1.1 Limitations

Not all subjects were processed, analysed and included in the grand averaging. In particular, the power spectral density of the excluded subjects shows a broad peak in the frequency range between 8 Hz and 12 Hz. In some, a second component is also present in the frequency range between 20 Hz and 24 Hz. The Figure 5.7 shows the power spectral density of subject 5 and it can be seen that the component in the frequency range between 8 Hz and 12 Hz is greater than the component in the frequency range between 20 Hz and 24 Hz. In particular, the presence of these frequencies influences the success of the jitter compensation algorithm. This algorithm aims, as described in the previous chapters, to compensate the variability in latency between the different trials by exploiting Pearson's linear correlation. Aligning the different trials, it results in an amplitude sum of these harmonic components that cause the signal to oscillate, causing distortion and the possibility of identifying characteristic component because the interfering component prevails over the signal.

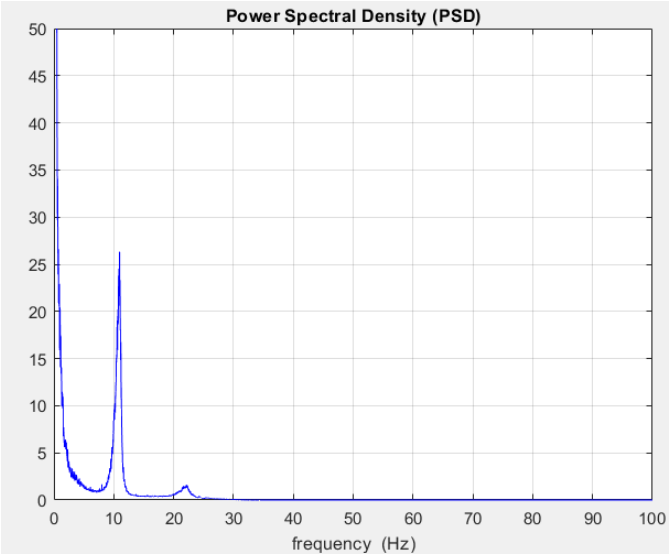

Figure 5.7: Subject 5: Power spectral density. The highest frequency peak is between 8 and 12 Hz. The second peak is between 20 and 24 Hz.

The Figure 5.8 and Figure 5.9 show the SEPs and the SNRs of the subject 5 in the two possible hand orientations. It can be observed that the signals do not present the expected waveform with the peaks described above. The SNRs trend are also not satisfactory. In the thumb palm-up condition in the time interval between 150 ms and 250 ms, the SNR is negative. Consequently, all subjects with these frequency components were excluded from the analysis.

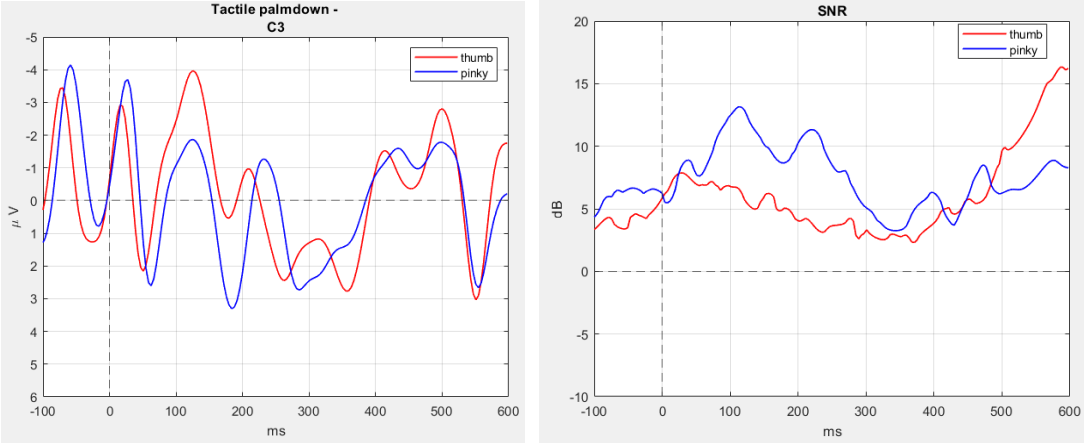

Figure 5.8: Palmdown condition: SEP and SNR of subject 5 (thumb in red and pinky in blue) obtained by re-referencing, temporal filtering, artefact correction algorithm, robust detrending, baseline correction methods and jitter compensation

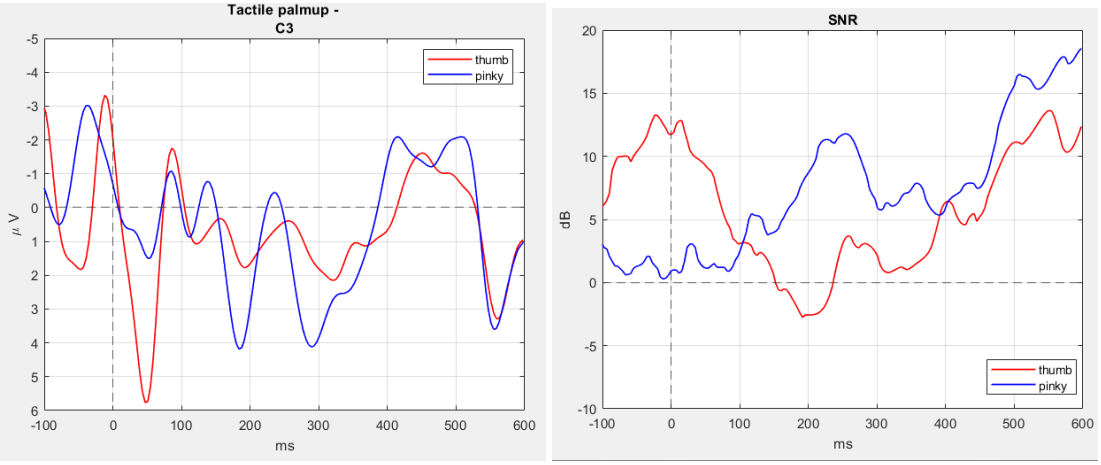

Figure 5.9: Palmup condition: SEP and SNR of subject 5 (thumb in red and pinky in blue) obtained by re-referencing, temporal filtering, artefact correction algorithm, robust detrending, baseline correction methods and jitter compensation

In the future, in order to solve this limitation of the plug-in, an additional step in the pre-processing chain could be introduced, as proposed in the literature [49], time-frequency filtering with wavelet analysis. This technique allows stimulus-related responses to be isolated and analysed from EEG background artefacts, and SNR to be improved.

5.2 Statistical analysis

To evaluate the validity of the results obtained, a statistical analysis was performed.

The *t-statistic*, or t-score, is a statistical test of significance to assess whether there is a significant difference between two groups. The t-statistic is used when the sample size is small, as is the case here, and it is desired to infer characteristics of a larger population from such samples, or when the standard deviation of the population is unknown. To assess the presence of a difference between two groups, the null hypothesis is formulated. In this context it is assumed as a null hypothesis that the signal has no peaks and that it is noise. If on the basis of the statistical test this hypothesis is accepted, the signal is noise, conversely if the null hypothesis is rejected then the peaks present in the signal are valid and are not noise. The random variable t is calculated as:

$$t = \frac{\bar{x} - \mu}{s/\sqrt{n}} \tag{5.1}$$

where $\bar{x}$ is the sample mean, μ is the hypothesised average of the population, s is the standard deviation of the sample and n is the sample dimension.
It indicates the distance, in terms of standard deviation, between the sample mean and the assumed population mean. To take into account the number of comparisons performed and to avoid many spurious values, the alpha value must be reduced. Considering that for a single comparison a certain alpha value may be appropriate, it is not adequate for the set of all comparisons. Therefore, when several statistical tests are performed simultaneously, the *Bonferroni correction* is used, which is a multiple comparison correction [50]. The alpha value in the Bonferroni correction is adjusted for the entire set of n comparisons as:

$$\alpha_{\text{Bonferroni}} = \frac{\alpha}{m} \tag{5.2}$$

where α is the level of statistical significance (0,05) and m is is the number of hypotheses (in this study it is the length of the signal in sample: 256).

In order to test the results against the null hypothesis, the *Iterative Amplitude Adjusted Fourier Transform (IAAFT)* was used. The IAAFT is a randomisation technique mainly used in time series analysis to generate surrogates. Non-parametric hypothesis tests can be performed on the temporal structure of the data because the surrogates are characterised by the same distribution and power spectrum of a given data set. The algorithm used is an iterative algorithm in which the power spectrum of the original time series is obtained via the Fourier transform. Then a random shuffling is performed; in order to destroy the time dependency

the values of the original time series are randomly rearranged. Then Amplitude Adjustment is performed so that the original signal and the obtained random series have the same distribution. In order to obtain the new time series, the inverse Fourier Transform is performed. The steps are performed until a certain accuracy defined by the residual discrepancy of the spectrum is reached [51]. In order to test the null hypothesis, surrogates were generated for each epoch of the signal under investigation, and averaged to obtain the corresponding SEP. The figure Figure 5.11 shows, as an example, the SEP of the original time series of the pinky touch with the palm-up and the SEP of the surrogates (in red) generated from each epoch. As can be seen, the generated signal has no peaks and represents the null hypothesis.

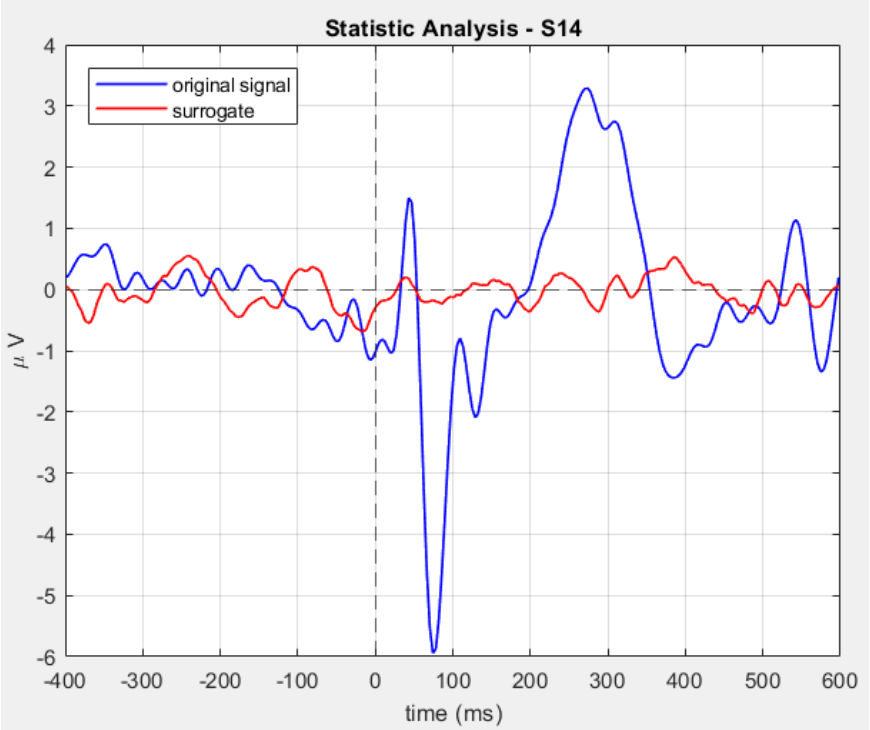

Figure 5.10: Illustration of the SEP of subject 14 in the pinky touch condition with the palm-up of the original time series (blue) and the SEP of the surrogates (red).

In order to assess the t-distribution of the null hypothesis, 10000 groups were created, each consisting of two subgroups made up of 50% randomly selected epochs from the original signal and 50% from epochs selected from the surrogate epochs. The total number of epochs was equal to those of the original signal. For each group, the t-statistic was assessed according to the Equation 5.1 where: the numerator

is defined by the difference of the averages of the subgroups of each group, the standard deviation is equal to the sum of the two standard deviations of the two subgroups and n is the number of the samples - 256 samples - of the signal.

The t-statistic of the signal with respect to the null hypothesis (SEP obtained from surrogates) was also evaluated according to the Equation 5.1, where $\bar{x}$ is is the average of the epochs of the original signal, μ is the average of the surrogate epochs, s is the standard deviation of the sum of the two signals and n is the number of the samples - 256 samples - of the signal.

Subsequently, using Bonferroni's alpha, it was evaluated whether the null hypothesis was accepted or rejected. In particular it was assessed whether the t-statistic of the signal was greater than the thresholds. If it was then the alternative hypothesis was confirmed and therefore the peaks were true and were not noise. Conversely if the t-statistic of the signal was less than the alpha, then the null hypothesis was confirmed.

This procedure was performed for the thumb and little finger separately and for each condition (palm-up and palm-down).

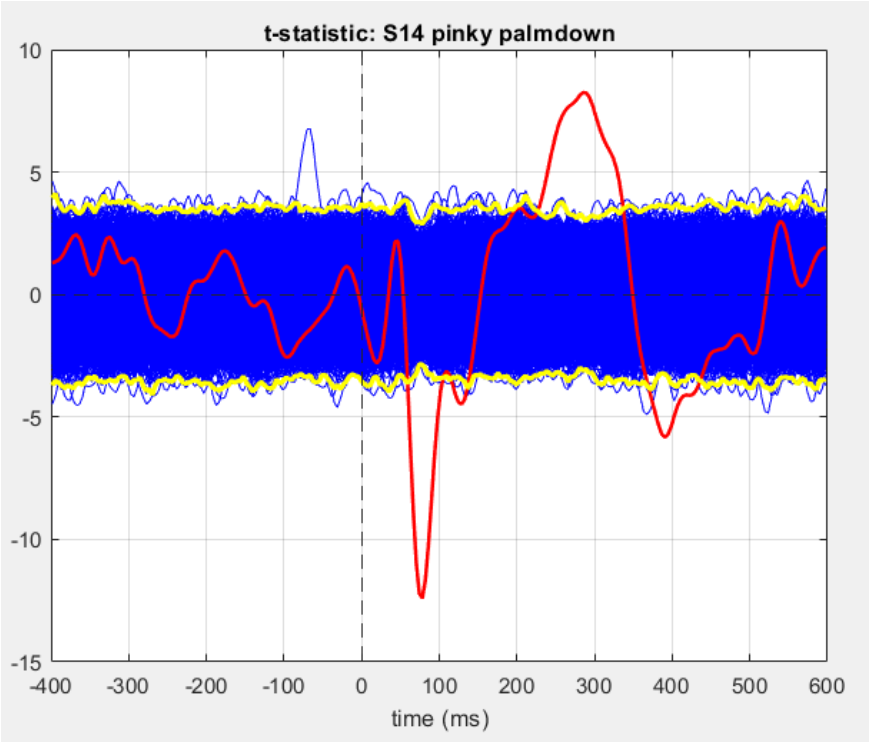

Figure 5.11: Illustration of the t-statistic of subject 14 of the palm-down pinky touch. The statistical distribution of the null hypothesis is shown in blue, the t-statistic of the signal is in red, and in yellow the thresholds determined by Bonferroni correction. The valid peaks are within the following time ranges: 58.6-105.5 ms (N80), 113.3-136.7 ms (N140) and 226.5-339.8 ms (P300).

Once the valid peaks had been identified for each subject, the peak of each component of interest (P45, N80, N140, P300) was identified on the grand averaging SEP. Once the peak of each was identified, a time range of 10 ms before the peak and 10 ms after the peak was considered as a reference. It was then assessed whether or not there was an intersection between the time range taken as a reference and the time range of the valid peaks of each subject. Below there are plots for each condition in which the identified reference time ranges and their respective tables are shown. The tables show for each analysed subject the time ranges of the valid peaks identified with the t-statistic and those that do not intersect the reference range have been marked in red.

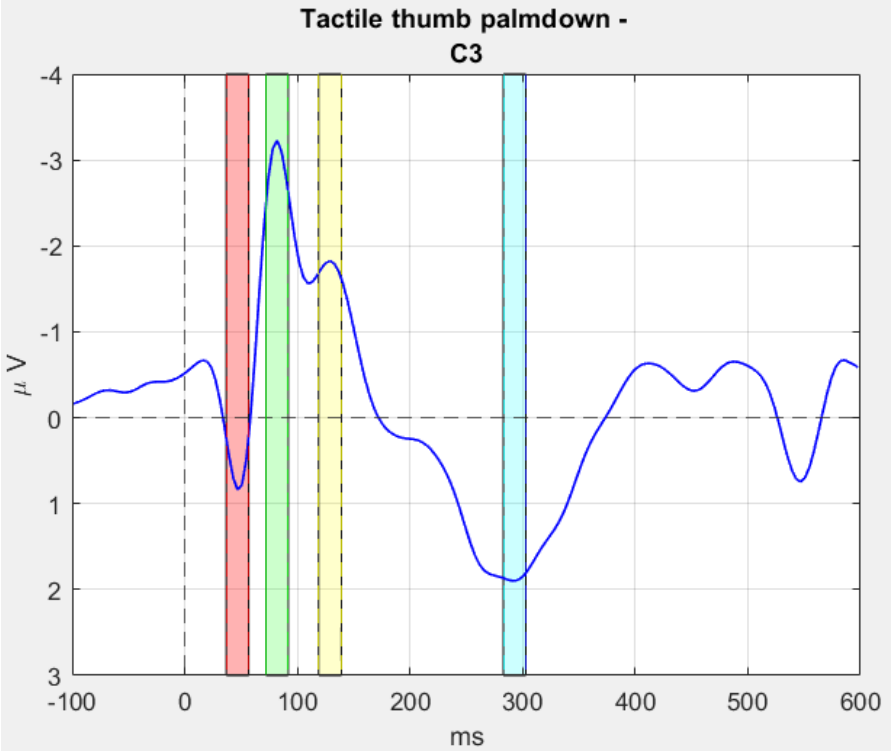

Figure 5.12: Illustration of the SEP of grand averaging for touch on the palm-down thumb. The reference time ranges for each component are highlighted in different colours (P45 - red, N80 - green, N140 - yellow, P300 - blue).

THUMB PALM-DOWN				
Subject	**P45**	**N80**	**N140**	**P300**
Peaks	46.8 ms	82 ms	128.9 ms	292.9 ms
Range time	36.8-56.8 ms	72-92 ms	118.9-138.9 ms	282.9-302.9 ms
S1	39-66 ms		125-136 ms	277-320 ms
S2		66-89 ms		261-308 ms
S4	39-51 ms	62-137 ms		
S6	42-54 ms	70-136 ms		
S9	35-62 ms	70-109 ms	128-195 ms	382-402 ms
S14		58-93 ms		234-324 ms
S19		58.5-156.3 ms		277-398 ms
S24	35-66 ms	66-160 ms		234-363 ms
S25		58-156 ms		300-351 ms
S27	19-62 ms	62-156 ms		265-300 ms
S30	42-70 ms		121-148 ms	
S34		70-101 ms	128-152 ms	234-332 ms
S40		68-82 ms		242-289 ms

Table 5.1: Summary table of subjects in the thumb touch palm-down condition. There is no intersection between the reference range of the P300 and the time range of subjects 9, 25 and 40 for the P300.

Figure 5.13: Illustration of the SEP of grand averaging for touch on the palm-down pinky. The reference time ranges for each component are highlighted in different colours (P45 - red, N80 - green, N140 - yellow, P300 - blue).

PINKY PALM-DOWN				
Subject	**P45**	**N80**	**N140**	**P300**
Peaks	46.8 ms	82 ms	128.9 ms	292.9 ms
Range time	36.8-56.8 ms	72-92 ms	115-135 ms	286.8-306.8 ms
S1	39-66 ms		121-137 ms	300-328 ms
S2		66-93 ms	101-125 ms	
S4		62.5-121.1 ms		
S6	39-62 ms	66.4-132.8 ms		
S9	39-62.5 ms	66.4-121.1 ms		269.5-400 ms
S14		58.6-105.5 ms	113.3-136.7 ms	226.5-339.8 ms
S19		62.5-140.6 ms		339.8-371.1 ms
S24	39.1-54.7 ms	70.3-156.3 ms		253.9-339.8 ms
S25		62.5-140.6 ms		
S27	31.2-58.6 ms	70.3-132.8 ms		199.2-222.6 ms
S30	42.9-74.2 ms		160.1-171.8 ms	
S34		74.2-156.2 ms		226.6-316.4 ms
S40		70.3-125.1 ms		

Table 5.2: Summary table of subjects in the thumb touch palm-down condition. There is no intersection between the reference range of the P300 and the time range of subjects 1, 19 and 27 for the P300. For the subject number 30 there is no intersection between the ranges time for the N140 component.

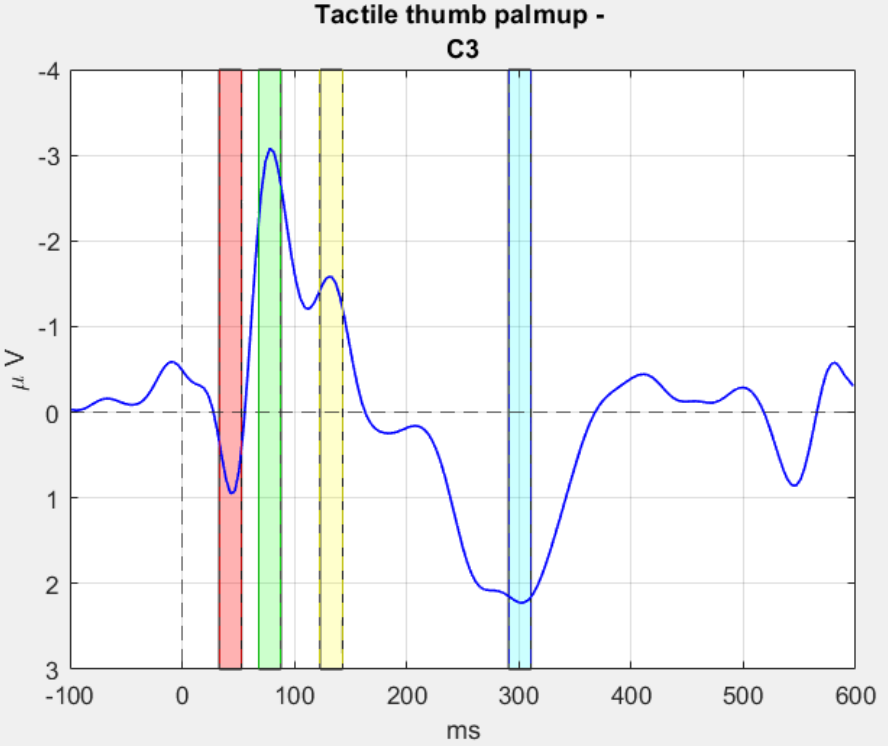

Figure 5.14: Illustration of the SEP of grand averaging for touch on the palm-up thumb. The reference time ranges for each component are highlighted in different colours (P45 - red, N80 - green, N140 - yellow, P300 - blue).

THUMB PALM-UP				
Subject	**P45**	**N80**	**N140**	**P300**
Peaks	42.9 ms	78.1 ms	132.8 ms	300.8 ms
Range time	32.9-52.9 ms	68.1-88.1 ms	122.8-142.8 ms	290.8-310.8 ms
S1	35.2-66.4 ms		121.1-144.5 ms	281.2-332 ms
S2		62.5-96.8 ms		259-316.4 ms
S4		66.4–136.7 ms		
S6	42.9-54.7 ms	70.3-144.5 ms		285.2-371.1
S9	42.9-58.6 ms	70.3-105.5 ms		
S14		58.6-101.6 ms		222.6-335.9 ms
S19		54.7-148.4 ms		273.4-406 ms
S24	31.3-58.6 ms		93.8-175.8 ms	246.1-335.9 ms
S25	31.3-50.8 ms	66.4-164 ms		328.2-351.6 ms
S27	35.2-54.7 ms	70.3-97.7 ms	148.4-174.8 ms	261.7-289.1 ms
S30	46.2-70.3 ms			
S34		70.3-113.21 ms		234.3-320.3 ms
S40		66-82 ms		234.3-265.6 ms

Table 5.3: Summary table of subjects in the thumb touch palm-up condition. There is no intersection between the reference range of the P300 and the time range of subjects 25, 27 and 40 for the P300.

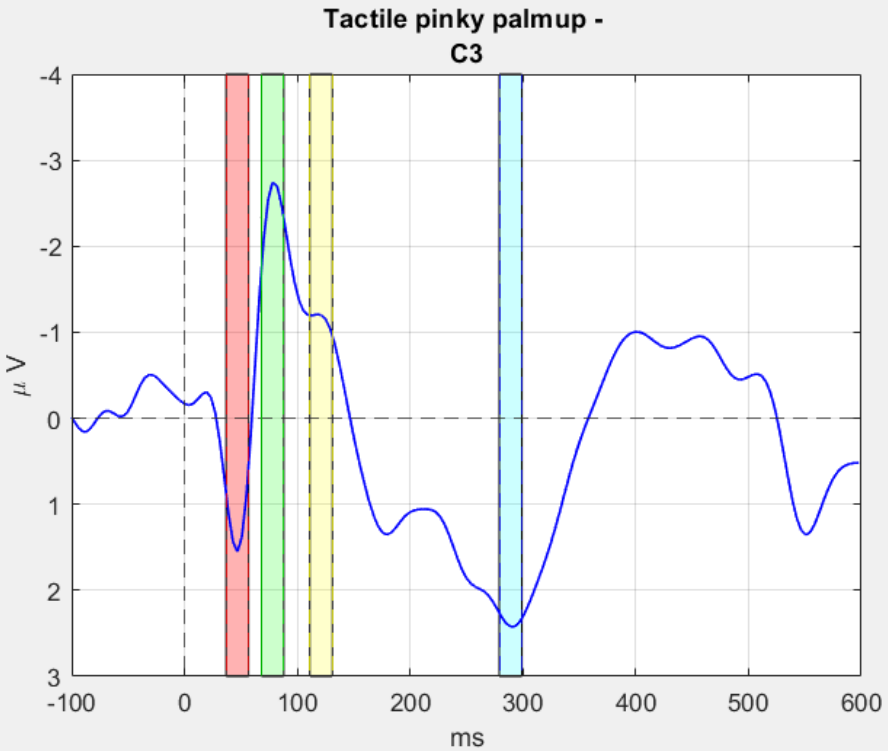

Figure 5.15: Illustration of the SEP of grand averaging for touch on the palm-up pinky. The reference time ranges for each component are highlighted in different colours (P45 - red, N80 - green, N140 - yellow, P300 - blue).

PINKY PALM-UP				
Subject	**P45**	**N80**	**N140**	**P300**
Peaks	46.9 ms	78.1 ms	121.1 ms	289.1 ms
Range time	36.9-56.9 ms	68.1-88.1 ms	111.1-131.1 ms	279.1-299.1 ms
S1	39-62.5 ms		105.5-148.4 ms	269.5-328.1 ms
S2		65.5-89.8 ms		261.7-300 ms
S4		60-85.9		296.7-316.4 ms
S6		66.4-141 ms		187.5-328.1 ms
S9	35.2-66.4 ms		85-121 ms	281-308 ms
S14		62.5-101.5 ms		214-316.4 ms
S19		66.4-148.4 ms		269.5-375 ms
S24	35.2-58.6 ms	70.3-148.4 ms		175.7-343.7 ms
S25		58.6-140.6 ms		179.7-277.3 ms
S27	39.1-50.8 ms	66.4-121.1 ms		281.3-304.7 ms
S30	42.9-58.6 ms			289-335.9 ms
S34		74.2-148.4 ms		242.2-342.7 ms
S40		71-127.3 ms		

Table 5.4: Summary table of subjects in the thumb touch palm-down condition. There is no intersection between the reference range of the P300 and the time range of subjects 4 and 25.

The results show that the valid components at P45 and N80, identified in the subjects for all touch conditions via the t-statistic, all intersect the respective reference time ranges. In contrast, for component N140 in only two conditions do they not intersect the reference time range, in subject 30 in the palm-down pinky touch and in subject 27 in the palm-up thumb touch. A larger number of components at P300 do not intersect the reference time range: subject 9 in palm-down thumb touch, subject 25 in both the palm-up touch orientation condition and the palm-up pinky touch condition, subject 27 in the palm-down pinky touch and palm-up thumb touch condition, subject 40 in both the palm-up touch conditions, subject 1 and 19 in palm-down pinky touch and subject 4 in palm-up pinky touch.

Bonferroni correction can be very conservative and reduce statistical power, so *cluster-based statistic* could be used in the future. This statistic offers a robust approach to tackle the problem of multiple comparisons, improving the interpretation and reliability of results compared to Bonferroni correction. Cluster-based statistic is a multivariate data analysis technique aimed at selecting and grouping homogeneous elements in a data set, reducing the risk of false positives that can occur when testing individual data points separately. It makes it possible to identify regions of interest in spatial and temporal data without having to apply multiple

test corrections to each data point individually.

To assess any difference between the touch on the thumb and the little finger in the two different conditions, the *Wilcoxon Rank Sum test* was performed, a non-parametric statistical test used to compare two independent samples. The Wilcoxon rank sum test is the equivalent of the Mann-Whitney U-test. It is also a non-parametric test and is used to check the equality of the population medians of two independent samples X and Y. The Mann-Whitney test statistic U indicates how often an element of sample y precedes an element of sample x when the elements of the two independent samples X and Y are arranged in order. It correlates with the Wilcoxon rank sum in the following way:

$$U = W - \frac{n\chi(n\chi + 1)}{2} \tag{5.3}$$

For implemented the Wilcoxon rank sum test was used the Matalab function *ranksum*. This function gives the p-value for a two-sided Wilcoxon rank sum test and a logical value indicating the test decision. The difference between of the touch on the same finger with the two different orientation of the hand is the null hypothesis. In the both cases the null hypothesis was reject (h=0), therefore there isn't different on the touch between the two orientation of the hand on the same finger.

Chapter 6

Vicarious touch

In this chapter, the vicarious touch will be introduced, as the data used to develop the plug-in were acquired to investigate, by means of time-resolved multivariate pattern analysis, whether there is an overlap of neural representations between seen touch and direct touch experience on EEG data acquired from people with and without vicarious touch experience. Furthermore, this chapter will introduce SEPs obtained by averaging trails with visual task, whereas in the previous chapters only SEPs obtained with the touch task were discussed.

6.1 Mirror touch

Vicarious touch, or *mirror touch*, refers to the automatic simulation of observed tactile sensations on another person's body. This phenomenon is associated with the activation of a broad somatosensory cortical network during the visual perception of touch [52]. Early imitative experiences involving multiple body senses promote emotional and motoric attunement between infants and their primary caregivers, leading to the development of a basic sense of self [53]. Mirroring is fundamental because it is the basis of our social being, i.e. an intuitive bodily resonance with others. In fact, when observing what happens to others we are able to understand what they are feeling but also empathise with their states. Studies conducted in Parma in the nineties showed that mirror neurons (some premotor neurons) are activated both during the execution of a movement and during observation of the same. The understanding of the neural basis of empathy was made possible by vicarious motor responses, whereby one could empathise with other people and observing them activated representations of corresponding states in our brain [52][54].

The vicarious experiences have neurophysiological foundations in the sensorimotor systems related to the adaptation of externally perceived events, such as

visual, and internally experienced, affective and sensory-motor. It has been shown with fMRI studies that the observation of touch gives rise to brain activity in the somatosensory SI and SII cortices, in fronto-parietal mirroring networks and also in the self-other distinction networks. The degree to which external stimuli are experienced as relative depends on the strength of the individual's attachment to his or her bodily self. In particular, when there is a stronger relationship with the self, behavioural responses are stronger in vicarious touch. It has been shown that in vicarious touch P45 is the most specific index of the relationship with the self. The neural activity of the primary somatosensory cortex is mirrored in the P45 component, consequently vicarious touch modulates SI. Vicarious touch has been shown to be influenced by the perspective of the viewed hand. To assess tactile empathy, the *tactile mirroring paradigm* is used, in which subjects observe a second person's body being touched or not and simultaneously receive the tactile stimulus on the hidden part of their own body. An internal simulation of the observed event is induced by mirroring. When touch is observed, there must be a correspondence between the representations of the stimulus felt and seen, and there must not be when non-touch is observed. Through the difference in somatosensory processing between touch and non-touch conditions, the effect of vicarious touch is assessed [54].
In this thesis project, the tactile mirroring paradigm could not be used because the visual and tactile stimuli were provided separately. Below there are the results of the subjects' averaging of the visual stimulus.

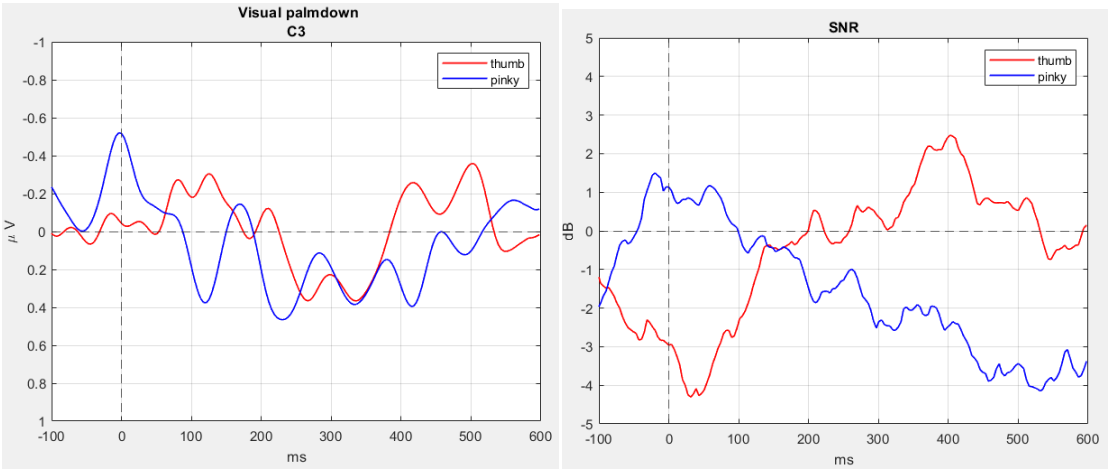

Figure 6.1: Palm-down condition with visual stimulus: SEP and SNR of the average between subjects (thumb in red and pinky in blue) obtained by re-referencing, temporal filtering, artefact correction algorithm, robust detrending, baseline correction and jitter compensation methods.

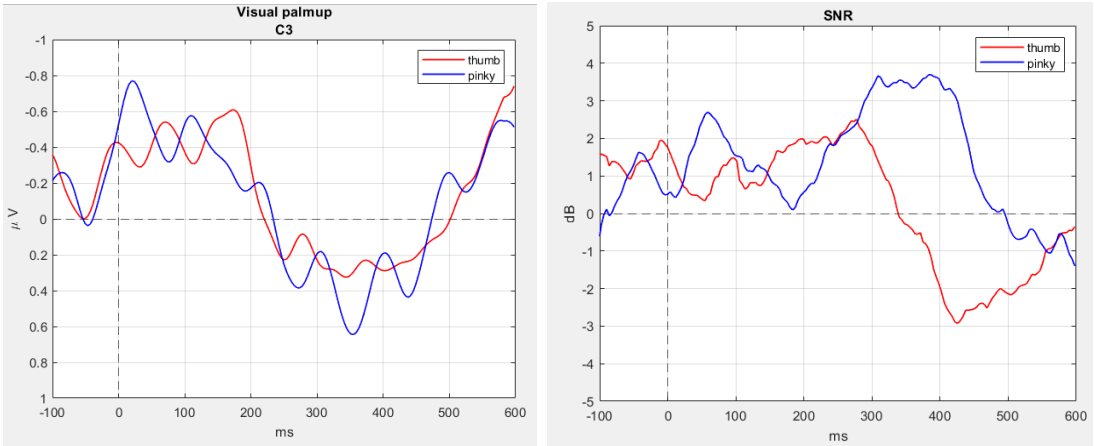

Figure 6.2: Palm-up condition with visual stimulus: SEP and SNR of the average between subjects (thumb in red and pinky in blue) obtained by re-referencing, temporal filtering, artefact correction algorithm, robust detrending, baseline correction and jitter compensation methods.

In figure Figure 6.1 and Figure 6.2, the SEPs and the SNRs of the average of the subjects after applying the following pre-processing are shown: re-referencing, temporal filtering, artefact correction algorithm, robust detrending, baseline correction and jitter compensation algorithm. It can be observed that the signals are very noisy, the SNR of the visual stimulus to the little finger in the palm-down condition assumes a value close to zero in the time interval from the onset of the stimulus to 100 ms and to become less than zero. In contrast, for the visual stimulus on the thumb, in the same condition, it is negative up to about 150 ms and then increases slightly above 0. The same observations can be made for the palm-up condition even though the SNR is greater than 0 for most of the epoch duration, but it is very low.

Higher quality measurements could be collected and the touch condition could be included in the acquisition protocol while the tactile stimulus is shown on the screen, in order to be able to perform vicarious touch analysis according to the tactile mirroring paradigm.

Furthermore, in the future, it could be possible to evaluate the rhythm *mu* through frequency analysis. *Mu waves* have a frequency similar to that of α waves, but differ in location. They are mainly localised in the central areas of the brain (in the motor regions of the cerebral cortex). They are related to attention and motor activity. The *mu* rhythm is reduced during voluntary movement of a body's part

or when the subject observes someone else performing the same action. This is called mu blockade and is related to the activity of mirror neurons.

Chapter 7

Conclusions

This thesis focuses on the development of an EEGLab plug-in for the calculation of Somatosensory Evoked Potentials. The pre-processing chain for EEG data was implemented with the following steps: re-referencing, temporal filtering, artifacts corrections with Independent Component Analysis (ICA), epoching, baseline correction, jitter compensation, and extrapolation of SEPs with the averaging technique.

The application of re-referencing, temporal filtering, artifact correction, robust detrending, and baseline correction methods significantly improved the Signal-to-Noise Ratio and the shape of the SEPs.

Jitter compensation algorithm further improved SEP signal quality by compensating for process-to-process latency variability. It improved the amplitude of the signal components and the signal-to-noise ratio. The improvements were more pronounced under some conditions than others, demonstrating the effectiveness of this technique in different experimental setups.

After pre-processing the EEG signal, high quality SEPs are obtained and characteristic components can be identified: P45, N80, N140 and P300. The components reflect different levels of processing of the tactile stimulus. The P45 is the early component that identifies the moment at which the brain recognises the tactile stimulus.

By averaging the SEPs of multiple subjects, the influence of individual variations in electrophysiological characteristics, physiology and anatomy was reduced. This approach not only improved the signal of interest, but also increased the validity and statistical power of the results, making the data analysis more robust and reliable.

The statistical analysis conducted confirmed the reliability of the pre-processing chain implemented. The results indicated a significant improvement in the SNR,

which is crucial for accurately interpreting the SEP data.

Bibliography

[1] American Association of Neurological Surgeons. «Anatomy of the Brain». In: (2023). URL: https://www.aans.org/en/Patients/Neurosurgical-Conditions-and-Treatments/Anatomy-of-the-Brain (cit. on pp. 1, 3, 5).

[2] T. Hines. «Anatomy of the Brain». In: *Mayfield Clinic* (2018). URL: https://mayfieldclinic.com/pe-anatbrain.htm (cit. on pp. 1–3, 5).

[3] Johns Hopkins Medicine. «Brain Anatomy and How the Brain Works». In: (2023). URL: https://www.hopkinsmedicine.org/health/conditions-and-diseases/anatomy-of-the-brain (cit. on pp. 2, 5).

[4] L. Hampton and J. Costa. «Cerebral Cortex». In: *Physiopedia* (). URL: https://www.physio-pedia.com/Cerebral_Cortex (cit. on p. 3).

[5] «Primary Somatosensory Cortex». In: *The Human Memory* (2022). URL: https://human-memory.net/primary-somatosensory-cortex/ (cit. on p. 3).

[6] «La corteccia somatosensoriale – Introduzione alla Psicologia». In: *State of Mind* (). URL: https://www.stateofmind.it/2018/01/corteccia-somatosensoriale/ (cit. on pp. 4, 5).

[7] «Homunculus». In: *Neuropsycholoy* (). URL: http://www.neuropsychology.it/voce_glossario.asp?idglossario=248 (cit. on pp. 4, 5).

[8] «Homunculus». In: *Britannica* (). URL: https://www.britannica.com/science/heredity-genetics (cit. on p. 4).

[9] «Brain Basics: The Life and Death of a Neuron». In: *National Institute of Neurological Disorders and Stroke* (2023). URL: https://www.ninds.nih.gov/health-information/public-education/brain-basics/brain-basics-life-and-death-neuron (cit. on pp. 6, 7).

[10] «Nerve Tissue». In: *National Cancer Institute* (). URL: https://training.seer.cancer.gov/anatomy/nervous/tissue.html (cit. on p. 7).

[11] «Neurons: How the Brain Communicates». In: *Menatal Health America* (). URL: https://mhanational.org/neurons-how-brain-communicates (cit. on p. 7).

[12] «The Neuron». In: *BrainFact.org* (2012). URL: https://www.brainfacts.org/brain-anatomy-and-function/anatomy/2012/the-neuron (cit. on p. 7).

[13] «Neurons». In: *Organismal Biology* (). URL: https://organismalbio.biosci.gatech.edu/chemical-and-electrical-signals/neurons (cit. on p. 8).

[14] J Lee and P. Clavo. «The potential of plant action potentials». In: *Synthese* 202 (Nov. 2023) (cit. on pp. 8, 9).

[15] «Action potentials and synapses». In: *The university of queensland* (). URL: https://qbi.uq.edu.au/brain-basics/brain/brain-physiology/action-potentials-and-synapses (cit. on pp. 8–10).

[16] Jeffrey W Britton, Lauren C Frey, Jennifer L Hopp, Pearce Korb, Mohamad Z Koubeissi, William E Lievens, Elia M Pestana-Knight, and Erk K St Louis. «Electroencephalography (EEG): An introductory text and atlas of normal and abnormal findings in adults, children, and infants». In: (2016) (cit. on pp. 11, 14).

[17] K. Blinowska and P. Durka. «Electroencephalography (EEG)». In: *Wiley encyclopedia of biomedical engineering* (2006) (cit. on pp. 11, 12, 15, 16, 18, 19).

[18] F. Carpi and D. De Rossi. «Fenomeni bioelettrici». In: (Cap. 17) (cit. on pp. 11, 14).

[19] N. Bajaj. «Wavelets for EEG Analysis». In: *Wavelet Theory*. IntechOpen, 2020. Chap. 5 (cit. on pp. 12, 13).

[20] «I potenziali evocati (ERP): in cosa consistono – Introduzione alla Psicologia». In: *State of Mind* (). URL: https://www.stateofmind.it/2017/09/potenziali-evocati/ (cit. on pp. 14, 15).

[21] M.H. Coles and M.D. Rugg. «Electrophysiology of mind: Event-Related Brain potentials and Cognition». In: *Oxford University Press* (1996) (cit. on p. 15).

[22] S.J Luck. «An introduction to event related potentials and their neural origins». In: *An introduction to the event related potential technique* 11 (2005) (cit. on p. 15).

[23] S. Shravani and V.K. Sinha. «Event-related potential: An overview». In: *Industrial psychiatry journal* 18 (2009), pp. 70–73 (cit. on p. 16).

[24] X. Lu and L Hu. «Electroencephalography, Evoked Potentials, and Event-Related Potentials». In: *EEG Signal Processing and Feature Extraction*. Springer Singapore, 2019, pp. 23–42 (cit. on p. 17).

[25] M.J. Aminoff and D.S. Goodin. «Visual Evoked Potentials». In: *Journal of Clinical Neurophysiology* 11.5 (Sept. 1994), pp. 493–499 (cit. on p. 17).

[26] A.J. Fowle. «Clinical neurophysiology». In: *Medicine* 48.8 (2020), pp. 550–554 (cit. on pp. 18, 19).

[27] J.L. Carte and J.C. Stevens. «Somatosensory Evoked Potentials». In: *Clinical Neurophysiology*. Oxford Academic, Apr. 2009, pp. 257–280 (cit. on pp. 19, 22, 24).

[28] M.J Aminoff and A.A Eisen. «AAEM MINIMONOGRAPH 19:SOMATOSENSORYEVOKED POTENTIALS». In: *Muscle Nerve* 21.3 (1998), pp. 277–290 (cit. on p. 20).

[29] I. Hashimoto, K. Yoshikawa, and M. Sasaki. «Latencies of peripheral nerve and cerebral evoked electrical stimul». In: *Muscle Nerve* 13.12 (1990), pp. 277–290 (cit. on p. 20).

[30] G. Crucco and at al. «Recommendations for the clinical use of somatosensory-evoked potentials». In: *Clinical Neurophysiology* 119 (2008), pp. 1705–1719 (cit. on pp. 20, 22).

[31] D. at al Purves. «Neuroscience, 3rd ed.» In: Sinauer Associates, 2004 (cit. on p. 21).

[32] American Clinical Neurophysiology Society. «Guideline 9D: Guidelines on Short-Latency Somatosensory Evoked Potentials». In: *Arch Neurol* 40(4) (1983), pp. 215–220 (cit. on p. 22).

[33] Colonm E.J. and G. Comi. «Long latency somatosensory evoked potentials». In: *Evoked Potential Manual: A Practical Guide to Clinical Applications*. Springer Netherlands, 1990, pp. 279–306 (cit. on pp. 22, 23).

[34] T Yamada, J. Kimura, J.T. Wilkison, and Kayamori R. «Short- and long-latency median somatosensory evoked potentials. Findings in patients with localized neurological lesions». In: *Journal of clinical neurophysiology* 23(2) (2006), pp. 168–179 (cit. on p. 22).

[35] A. Eisen. «The Somatosensory Evoked Potential». In: *Le journal C anadien des sciences neurologiques* 9(2) (1982), pp. 65–77 (cit. on p. 24).

[36] S. Smit, D. Moerel, R. Zopf, and A.N. Rich. «Vicarious touch: overlapping neural patterns between seeing and feeling touch». In: *NeuroImage* 278 (2023), p. 120269 (cit. on pp. 25, 26, 28, 29).

[37] «What is EEGLAB». In: *Swarts center for Computational Neuroscience* (). URL: `https://sccn.ucsd.edu/eeglab/index.php` (cit. on p. 30).

[38] C. Brunner, A. Delorme, and S. Makeig. «EEGLAB - An Open Source Matlab Toolbox for Electrophysiological». In: *Biomedical Engineering / Biomedizinische Technik* 58 (2013) (cit. on p. 30).

[39] A. De Cheveigné and D. Arzounian. «Robust detrending, rereferencing, outlier detection, and inpainting for multichannel data». In: *NeuroImage* 109 (2016), pp. 9–20 (cit. on pp. 33, 41–44).

[40] M. Makeig and S.A. Hillyard. «ERP Features and EEG Dynamics: An ICA Perspective». In: *Oxford Handbook of Event-Related Potential Components* (2009) (cit. on pp. 36, 37, 39).

[41] S.J. Luck. «An introduction to the event-related potential technique». In: *The MIT Press* (2014) (cit. on p. 37).

[42] Cristina Del Prete. «Enhancements of EEG Artifact Automatic Correction Algorithm and Processing of Hemiplegic Patients' EEG». In: *M. Eng, thesis. Politecnico di Torino* (March 2023) (cit. on pp. 37, 38).

[43] J. Van Driel, C.N.L. Olivers, and J.J Fahrefort. «High-pass filtering artifacts in multivariate classification of neural time series data». In: *Journal of Neuroscience Methods* 352 (2021), p. 109080 (cit. on pp. 44, 45).

[44] G. Ouyang, W. Sommer, and C. Zhou. «A toolbox for residue iteration decomposition (RIDE)—A method for the decomposition, reconstruction, and single trial analysis of event related potentials». In: *Journal of Neuroscience Methods* 250 (2015), pp. 7–21 (cit. on p. 46).

[45] G. Ouyang, W. Sommer, and C. Zhou. «Reconstructing ERP amplitude effects after compensating for trial-to-trial latency jitter: A solution based on a novel application of residue iteration decomposition». In: *International Journal of Psychophysiology* 352 (2021), p. 109080 (cit. on p. 47).

[46] A. Cabasson and O. Meste. «Time Delay Estimation: A New Insight Into the Woody's Method». In: *IEEE SIGNAL PROCESSING LETTERS* 15 (2008), pp. 573–576 (cit. on pp. 47, 48).

[47] Woody C.D. «Characterization of an adaptive filter for the analysis of variable latency neuroelectric signals». In: *Medical and biological engineering* 5 (1967), pp. 539–554 (cit. on p. 48).

[48] A. Manhães and A. França. «Event-related brain potentials (ERP): an overview». In: *Semantic scholar* (2011) (cit. on p. 53).

[49] L. Hu, Z.G. Zhang, Y.S. Hung, Luk K.D.K., G.D. Innetti, and Y Hu. «Single-trial detection of somatosensory evoked potentials by probabilistic independent component analysis and wavelet filtering». In: *Clinical Neurophysiology* 122 (2019), pp. 1429–1439 (cit. on p. 64).

[50] Eric W. Weisstein. «Bonferroni Correction». In: *MathWorld-A Wolfram Web Resource.* (). URL: `https://mathworld.wolfram.com/BonferroniCorrection.html` (cit. on p. 65).

[51] T. Schreiber and A. Schmitz. «Improved Surrogate Data for Nonlinearity Tests». In: *Physics Department, University of Wuppertal, D-42097 Wuppertal, Germany* (Feb. 1996) (cit. on p. 66).

[52] C. Keysers and Gazzola V. «Expanding the mirror: vicarious activity for actions, emotions, and sensations». In: *Neurobiology* 19 (Oct. 2019), pp. 666–671 (cit. on p. 78).

[53] V. Gallese and C. Sinigaglia. «The bodily self as power for action». In: *Neuropsychologia* 48 (Feb. 2010), pp. 746–755 (cit. on p. 78).

[54] J. Alder and H. Gillmeister. «Bodily self-relatedness in vicarious touch is reflected at early cortical processing stages». In: *Psichophysiology* (July 2019) (cit. on pp. 78, 79).